CHALMERS

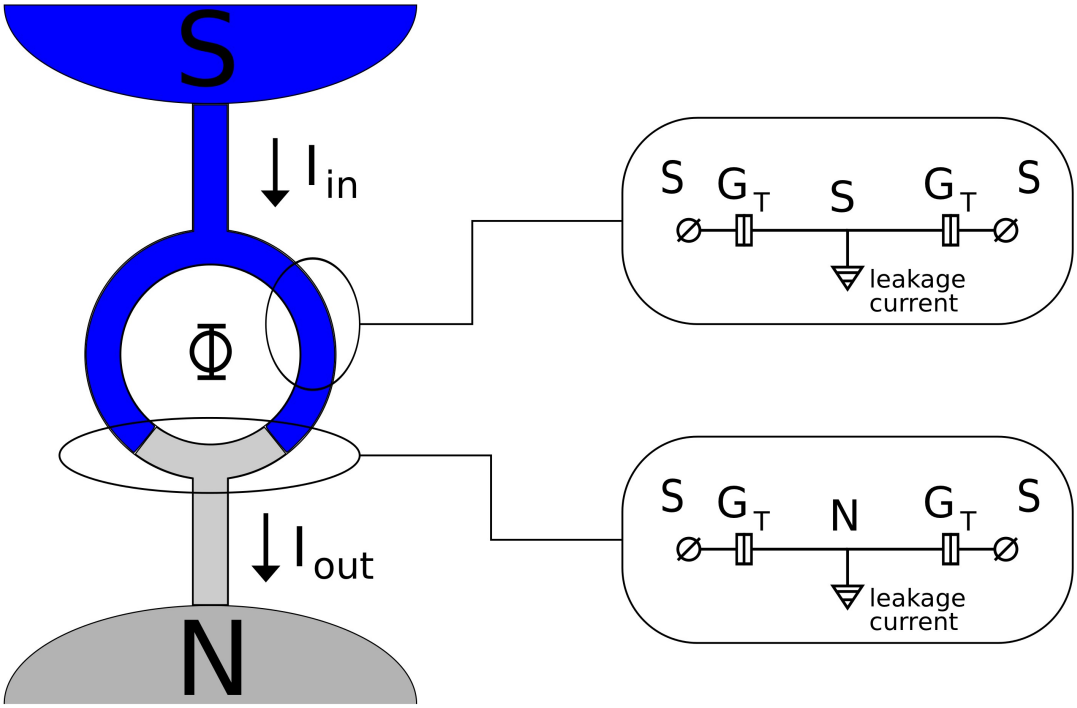

Circuit Theory of Mesoscopic Superconducting Components

Master of Science Thesis in Nanoscale Science and Technology

IAN KELLETT

Department of Microtechnology and Nanoscience
CHALMERS UNIVERSITY OF TECHNOLOGY
Göteborg, Sweden 2011

Circuit Theory of Mesoscopic Superconducting Components

IAN G. KELLETT

Department of Microtechnology and Nanoscience
CHALMERS UNIVERSITY OF TECHNOLOGY
Göteborg, Sweden 2011

Circuit Theory of Mesoscopic Superconducting Components
IAN G. KELLETT

Department of Microtechnology and Nanoscience
Chalmers University of Technology
SE-412 96 Göteborg, Sweden
Telephone +46 (0)31-772 1000

Cover: The illustration shows an Andreev interferometer and how SNS and SSS types of Josephson junctions arise when discretising the circuit for quantum circuit theory. The SNS junctions are discussed in section 5.1 and the SSS type is described in section 5.3.

Chalmers Reproservice
Göteborg, Sweden 2011

Circuit Theory of Mesoscopic Superconducting Components
IAN G. KELLETT
Department of Microtechnology and Nanoscience
Chalmers University of Technology

Abstract

Nazarov's quantum circuit theory is essentially a discretised version of the Usadel equation which describes mesoscopic superconducting systems in the diffusive limit.The focus of this thesis project was to investigate the application of the quantum circuit theory to an Andreev interferometer.

The report begins with a review of classical transport theory and then of the full Green's function theory of superconductivity leading to the Usadel equation. Quantum circuit theory is then presented with classical circuit theory as an analogy.

Quantum circuit theory is then applied to the SNS and SS'S type Josephson junctions that result when discretising the Andreev interferometer. Two types of SNS junctions were considered: firstly, an STNTS type with very strong tunnel junctions separating the intermediate metal from the reservoirs, and secondly, the short, diffusive SNS junction considered by Kulik-Omel'yanchuk. Finally, the added difficulties of a superconducting intermediate metal in the SS'S type junction are discussed and resolved.

Keywords: quantum circuit theory, Usadel equation, mesoscopic superconductivity, Josephson junction, Andreev interferometer

Acknowledgements

My time as a master's student is now at its end.
To give thanks would be prudent for I've had many a friend.

Mikael I thank for all the guidance I needed.
In Keldysh and Nambu spaces,
Thesis defence rooms amongst other places,
Your help has left me far from defeated,
Though my hair may have slightly receded.

The coffee room has also led to a treat,
For some fruit takers and coffee drinkers,
Not many home bakers, but always great thinkers,
There did I meet.
'Twas the AQP group, a delightful bunch,
That I've got a hunch will eat more sushi for lunch.

Thanks also to my family for their love and support.
Skype is a good way for us to keep in touch,
But still every day I miss you so much.
It is a shame to be so very bort bort,
That we only meet via TCP or air-port.

And last but not least, min älskade Kristin.
Lärt känna hennes familj har jag lyckligtvis fått.
För all deras hjälp finns inget tillräckligt mått.
Jag älskar dig, Kristin, med kärlek så fin,
Och snart blir vi tre i denna familjen min!

Contents

Nomenclature

$[A \ominus B]$	Commutator based on $\otimes$: $A \otimes B - B \otimes A$
$[A]_{ij}$	ith row, jth column entry of the matrix A
β	Inverse temperature
$\boldsymbol{A}(X)$	Magnetic vector potential
$\boldsymbol{E}$	Electric field
$\boldsymbol{F}$	Force
$\boldsymbol{I}$	Current density
$\boldsymbol{j}$	Spectral current density
$\boldsymbol{p}, \boldsymbol{k}$	Momentum vector
$\boldsymbol{r}$	Spatial coordinate vector
$\boldsymbol{v}$	Velocity vector
$\check{\phi}$	Matrix phase
$\check{\Sigma}$	Self-energy
$\check{G}$	4x4 Green's function
$\check{G}^{(1)}$	Small anisotropic part of $\check{G}(\boldsymbol{R})$
$\check{I}$	Matrix current
$\check{I}_{lc}$	Leakage current
$\check{\boldsymbol{j}}$	Matrix current density
Δ	Superconducting order parameter
δ	Dirac delta function
ϵ	Quasiparticle excitation energy

$\hat{A}$	Advanced Green's functions
$\hat{G}$	Green's function in Nambu space
$\hat{H}$	Hamiltonian operator in Nambu space
$\hat{K}$	Keldysh Green's functions
$\hat{R}$	Retarded Green's functions (2x2 in Nambu space)
$\hat{T}$	Time ordering operator
$\hat{\mathcal{G}}^M$	Matsubara Green's function
λ	Coupling strength of attractive electron interaction
λ_F	Fermi wavelength
$\langle ... \rangle$	Average over directions of momentum, $\boldsymbol{p}$
μ	Chemical potential
ν	Density of states per spin degree of freedom
$\otimes$	Convolution over shared coordinates, as well as matrix multiplication
ϕ	Phase difference of Δ across a junction
ψ	Field operator
ρ	Volume charge density
σ	Conductivity
σ_N	Normal state conductivity
τ	Imaginary time
τ_P	Momentum relaxation time
$\tilde{U}_{imp}$	Impurity potential
$\varepsilon(X)$	non-interacting single particle energy operator
ξ_0	Coherence length at T=0
ξ_N	Coherence length in normal metal
ξ_p	Energy (momentum) relative to Fermi energy
ζ_n	Matsubara frequency
A	Cross-sectional area of wire

c_{imp}	Impurity concentration
D	Diffusion coefficient
E	Energy
e	Elementary charge
E_F	Fermi energy
f	Particle distribution function
$f^{(1)}$	Small anisotropic term of distribution function, f
f_L	Longitudinal mode of distribution function f
f_T	Transverse mode of distribution function f
g	Dimensionless parameter proportional to $G_T\xi_N^2/(\sigma_N AL)$
G_0	Green's function of a free particle
G_Q	Conductance quantum, $2e^2/h$
G_T	Tunnel conductance
I	Current
k_F	Fermi momentum
L	Length of junction
l	Impurity mean free path
T_c	Critical temperature of bulk superconductor
T_p	Transmission eigenvalue of channel p
$T_{c'}$	Critical temperature of intermediate metal in junction
V	Electric potential
V_i	Volume of node i
$W_{\boldsymbol{p},\boldsymbol{p}'}$	Scattering rate from $\boldsymbol{p}$ to $\boldsymbol{p}'$
$\tilde{T}$	Reverse time-ordering operator

Chapter 1

Introduction

1.1 Background

The crowning achievement of the first half-century of studies on superconductivity was the microscopic theory put forth by Bardeen, Cooper, and Schrieffer (BCS) in 1957 [1]. The key is that if electrons near enough the Fermi surface have a mutual *attraction* of any strength, the Fermi sea becomes unstable. The energetically favourable state for the system then has electrons near the Fermi surface in pairs known as *Cooper pairs* each with energy E_F, the Fermi energy. This opens a gap of size $2|\Delta|$ in the density of states of excitations to the system, where Δ is known as the superconducting order-parameter which characterises the superconducting state.

The methods used originally by BCS are sufficient for uniform, traslationally invariant superconductors. In order to include effects such as a spacially varying order-parameter, $\Delta(\boldsymbol{r})$, or to distinguish local from nonlocal effects, more general techniques are required [2]. Such techniques were developed initially by de Gennes, Gor'kov and others [3, 4, 5] and are largely based on Green's functions. These methods were further developed over the years to include many inhomogeneities, interfaces and constrictions and will be referred to in the following as "the full theory". Among these developments was the quasiclassical technique and the resulting Usadel equation [6] for the dirty limit from which Nazarov derived the "quantum circuit theory" of Andreev conductance [7]. Nazarov claims that the idea behind quantum circuit theory stemmed from the frequent discrepancy between the complexity of the quasiclassical theory and the triviality of its results. Indeed, quantum circuit theory reproduces many of the results of the full theory with comparative ease. The circuit theory was developed and extended by numerous authors (see [8] for references and review) to include a variety of different types of junctions and to remove the original low-energy restriction in [7].

Quantum circuit theory is essentially a discretisation of the Usadel equa-

tion. This discretisation, and, in fact, much of quantum circuit theory is analogous to the familiar classical circuit theory based on Kirchoff's rules and Ohm's law. The analogy is useful as it allows some intuition in applying quantum circuit theory. Another important advantage of the quantum circuit theory is that it is easily programmed on computer for calculations. Nazarov provides an algorithm described in [8] and [9]. This algorithm is the basis for many of the calculations done in this thesis work. The most familiar method of electric circuit analysis is to use Kirchoff's current rule in the circuit. One divides the circuit into elements that are easily characterised. One approximates that in the good conducting regions, the potential is constant and then applies standard equations to the elements carrying a large change in potential. Ohm's law, $I = V/R$, for a resistor of resistance R is probably the best known such equation, implying for instance that the current through the resistor is given by the change in potential across the resistor divided by R. This method is an approximation to the more general Laplace's equation $\nabla \cdot \boldsymbol{I} = 0$, which is itself a current conservation law.

These rules, alas, are derived for classical circuits so they do not apply to quantum circuits. Furthermore, inherently quantum mechanical effects such as Superconductivity, for instance, requires coherence between electrons and holes and so could never be incorporated in the framework above.

For circuits of conductivity on the order of a few conductance quanta $G_Q = 2e^2/h$ scattering matrix methods may be used to calculate transport properties. Otherwise, one uses Green's functions methods. Such methods lead to the Eilenberger equation and then in the Usadel equation for dirty systems. These equations are both discussed more later. They are solvable in some simple cases but even then are often much more complicated than the results [Nazarov book p.194] [1]. The Usadel equation, however, can be conveniently reformulated into a conservation equation, similar to the Laplace equation, and used as the basis for a quantum mechanical finite-element circuit theory analogous to the classical method above [Nazarov article 1999]. The method is can be used to obtain analytical results in some cases and is relatively straightforward to apply numerically. It is the primary method applied in this project work for studying nanostructures.

1.2 Motivation

The objective of the project was to model an Andreev interferometer as shown in figure 1.1 using quantum circuit theory. The approach of quantum circuit theory is to discretise a nanostructure into smaller, easily handled elements. Figure 1.1 shows also some of the building blocks of the Andreev interferometer arising from discretisation. A large part of this thesis focusses

[1] Unless otherwise indicated, the material discussed in this text is from Nazarov's book.

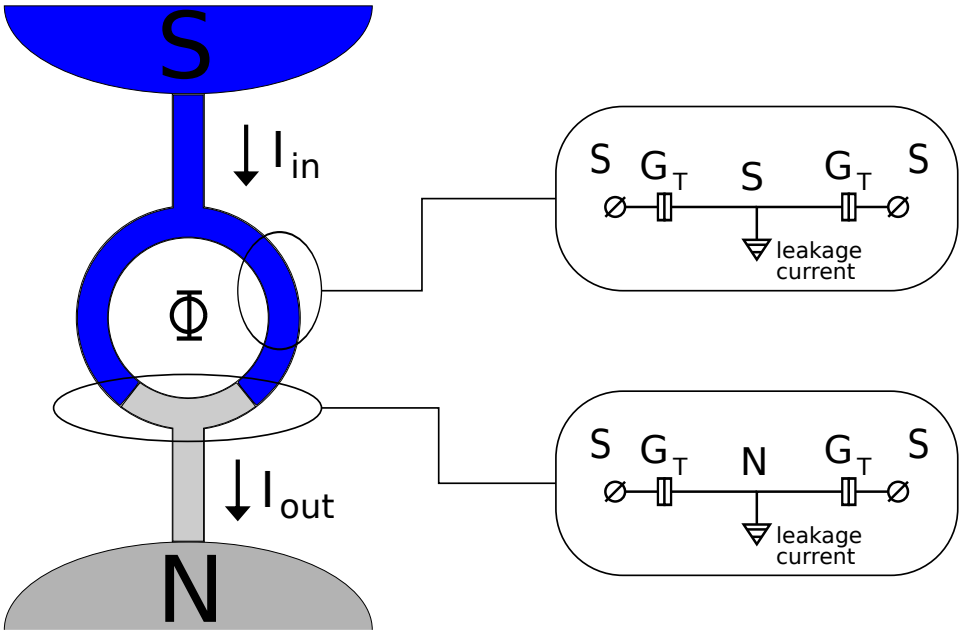

Figure 1.1: An illustration of an Andreev interferometer indicating the inherent presence of SNS and SSS type Josephson junctions that arise when discretising the circuit for calculation using quantum circuit theory. Such SNS and SSS type junctions were the focus of this thesis work because these cases can be extended to the full Andreev interferometer.

on these elementary structures. They serve as good stepping stones towards the full Andreev interferometer calculation using circuit theory.

1.3 Organisation of the report

This report begins with a review of the classical transport equations based on particle balance in chapter 2. This will serve as an analogy when the quantum circuit theory is presented. The full Green's function theory of superconductivity is then outlined in chapter 3. This results ultimately in the derivation of the Usadel equation. With the theoretical background established, quantum circuit theory is explained in chapter 4 in analogy with the classical circuit theory.

Chapter 5 then discusses the application of the circuit theory to the Superconducting-Normal-Superconducting (SNS) and SSS type Josephson junctions inherent in an Andreev interferometer. Two SNS-type scenarios are considered. The first such case is the STNTS type in which the intermediate normal metal is connected to the superconducting reservoirs by very strong tunnel junctions. The second case is a short, one dimensional

diffusive wire connecting the superconducting reservoirs. The results of the circuit theory analysis of the latter case are compared with the analytical results of Kulik and Omelyanchuk [10], referred to as the KO1 results. Having the superconducting intermediate metal in the SSS case requires additional care with the finite order-parameter, $\Delta(\boldsymbol{R})$. This is discussed and resolved in section 5.3.

Finally, conclusions from the thesis work and an outlook for future development in the area are given in chapter 6. Appendices supplementing the main text are provided in the end.

Chapter 2

"Classical" transport

The purpose of this chapter is to review important concepts of classical circuit analysis which are useful analogues for the quantum circuit theory presented in chapter 4. The chapter follows section 2.2 of [9] closely.

2.1 Boltzmann equation

To describe a statistical ensemble of many particles one uses a *distribution function*, $f(\mathbf{r}(t), \mathbf{p}(t))$, where $\mathbf{r}(t)$ and $\mathbf{p}(t)$ are position and momentum points in 6-dimensional phase space. The distribution function, $f(\mathbf{r}, \mathbf{p})$ gives the number of particles within a volume element dr^3dp^3 at position $\mathbf{r}$ and momentum $\mathbf{p}$. Since $\mathbf{r}$ and $\mathbf{p}$ change in time, the particles (and also the volume element) have the velocity $\mathbf{v}(\mathbf{p}) = \dot{\mathbf{r}}$ under the force $\mathbf{F}(\mathbf{r}) = \dot{\mathbf{p}}$. Ignoring scattering, the number of particles within the volume element is clearly fixed so

$$\frac{d}{dt} f(\mathbf{r}(t), \mathbf{p}(t)) = \frac{\partial f}{\partial t} + \boldsymbol{v}\frac{\partial f}{\partial \boldsymbol{r}} + \boldsymbol{F}\frac{\partial f}{\partial \boldsymbol{p}} = 0. \tag{2.1}$$

Impurities typically cause sharp potential profiles at a scale of k_F^{-1}. This enables the particles to scatter into states of different momentum, allowing for deviations of the distribution function, i.e. $\frac{df}{dt} \neq 0$. To account for scattering, one considers the scattering rates, $W_{\boldsymbol{p},\boldsymbol{p}'}$. The scattering rates are the probabilities of scattering from a state at $\boldsymbol{p}$ to a state at $\boldsymbol{p}'$ per unit time. Thus, the balance equation, eq. 2.1, becomes the Boltzmann equation for the non-equilibrium filling factor:

$$\frac{\partial f_{\boldsymbol{p}}}{\partial t} = -\boldsymbol{v}\frac{\partial f_{\boldsymbol{p}}}{\partial \boldsymbol{r}} - \boldsymbol{F}\frac{\partial f_{\boldsymbol{p}}}{\partial \boldsymbol{p}} + \int d\boldsymbol{p}(W_{\boldsymbol{p}',\boldsymbol{p}} f_{\boldsymbol{p}'} - W_{\boldsymbol{p},\boldsymbol{p}'} f_{\boldsymbol{p}'}),$$

with the notation $d\boldsymbol{p} = dp^3/(2\pi\hbar)^3$.

Quantum mechanics determines the scattering rates. Assuming low enough temperature (so that elastic scattering processes dominate), and

using the *Born approximation* and Fermi Golden rule one comes to an expression for the scattering rates:

$$W_{\boldsymbol{p},\boldsymbol{p}'} = \frac{c_{imp}}{\hbar}|\tilde{U}_{imp}(\boldsymbol{p}/\hbar - \boldsymbol{p}'/\hbar)|^2\delta(E(\boldsymbol{p}) - E(\boldsymbol{p}')).$$

$\tilde{U}_{imp}(\boldsymbol{p}-\boldsymbol{p}')$ is a Fourier component of the potential of an impurity and c_{imp} is the concentration of these impurities.

Supposing k_F^{-1} is much larger than the size of the impurities, then $\tilde{U}_{imp}$ does not depend on $\boldsymbol{k}$. This situation is called "white noise scattering" since the scattering potential is now seen as equal for all $\boldsymbol{k}$'s. The momentum relaxation time, $\tau_P^{-1} = (2\pi\nu c_{imp}/\hbar|U_{imp}|^2)$, now completely characterises the scattering. The symbol ν is the density of states per spin degree of freedom. The Boltzmann equation now becomes

$$\frac{\partial f}{\partial t} = -\boldsymbol{v}\frac{\partial f}{\partial \boldsymbol{r}} - \boldsymbol{F}\frac{\partial f}{\partial \boldsymbol{p}} + (\langle f\rangle - f)/\tau_P. \tag{2.2}$$

2.2 Drift diffusion equation

When the dimensions of a system are on a scale much larger than the mean free path, $l = v\tau_P$, the scattering of the electrons occurs so often that they "forget" their initial direction of momentum. This is the diffusive regime. In this case the distribution functions become essentially isotropic in $\boldsymbol{p}$. To observe the consequences on the Boltzmann equation given in eq. (2.2) a first approximation $f(\boldsymbol{r},\boldsymbol{p}) = f(E) + f^{(1)}(\boldsymbol{r},\boldsymbol{p})$ is useful, where $f^{(1)}$ is a small anisotropic part, $f(E) \gg f^{(1)}$, and $\left\langle f^{(1)}\right\rangle = 0$. This approximation in eq. (2.2) leads to

$$\frac{\partial f(E)}{\partial t} = -\boldsymbol{v}\frac{\partial f(E)}{\partial \boldsymbol{r}} - (\boldsymbol{F}\cdot\boldsymbol{v})\frac{\partial f(E)}{\partial E} - \frac{f^{(1)}}{\tau_P},$$

where $\boldsymbol{v} = \frac{\partial E}{\partial \boldsymbol{p}}$ and $\langle f(E)\rangle = f(E)$.

Taking the average of the original equation over all angles of the directions of $\boldsymbol{p}$ gives the *drift-diffusion equation*

$$\frac{\partial f(E)}{\partial t} = -\nabla\cdot\boldsymbol{j}, \tag{2.3}$$

where the spectral current density, $\boldsymbol{j}$, is temporarily defined as $\boldsymbol{j} = \left\langle \boldsymbol{v} f^{(1)}\right\rangle$ and will be renormalized later for convenience.

Taking the difference of the non-averaged and the averaged equations gives

$$-\frac{f^{(1)}}{\tau_P} = \boldsymbol{v}\frac{\partial f}{\partial \boldsymbol{r}} + (\boldsymbol{F}\cdot\boldsymbol{v})\frac{\partial f}{\partial E},$$

which provides an expression for the current density

$$\boldsymbol{j} = -D\boldsymbol{F}\frac{\partial f}{\partial E} - D\frac{\partial f}{\partial \boldsymbol{r}}, \tag{2.4}$$

where D is the diffusion coefficient. Multiplying eq. 2.4 by $e^2\nu$, the current density is now conveniently in units of conductivity, $\sigma = e^2\nu D$. Adopting this convention, the drift-diffusion equation becomes

$$e^2\nu\frac{\partial f}{\partial t} = -\nabla\cdot\boldsymbol{j}. \tag{2.5}$$

The current density is given by

$$\boldsymbol{I} = \int(\boldsymbol{j}/e)dE;\ \boldsymbol{j} = e^2\nu\left\langle \boldsymbol{v}f^{(1)}\right\rangle.$$

Usually ν, D and τ_P (and thus the conductivity σ also) vary on a scale of the Fermi energy. Electron transport happens, however, in a narrow range of energy, which is much smaller than the Fermi energy, at around the Fermi energy. As particle transport is the current focus, the values of ν, D and τ_P (and σ) may be replaced by their values at E_F. Integrating eq. 2.5 over energy then results in a simple conservation equation:

$$\frac{\partial\rho}{\partial t} = -\nabla\cdot\boldsymbol{I}\ ;\quad \boldsymbol{I} = \sigma\boldsymbol{E} - D\nabla\rho, \tag{2.6}$$

where $\rho = \int q\nu f(E)dE$, is the volume charge density. At low temperatures, states below E_F are generally filled and states above E_F are generally empty, the energy integral of $\delta f/\delta E$ can be approximated by $f(\infty) - f(0) = -1$.

Since all charges in metals reside at the surface, a good approximation is $\rho = 0$. Equation 2.6 then produces Laplace's equation together with Ohm's law:

$$\nabla\cdot\boldsymbol{I} = 0\ ;\quad \boldsymbol{I} = \sigma(\boldsymbol{r})\boldsymbol{E} = -\sigma(\boldsymbol{r})\nabla V. \tag{2.7}$$

These equations are the foundation for most basic circuit analysis.

Chapter 3

Semiclassical Transport

The classical approach to transport described above considers only particle balance, making no consideration of coherence between the particles. Of course, at quantum mechanical scales, coherence is important so that more rigorous methods are required. Green's functions methods (outlined briefly below) may provide a full description of the system of particles including the coherence but, in many cases, much of this information is superfluous and needlessly cumbersome mathematically. Some approximations, also outlined below, discard much of the extraneous information, leading to more easily handled *semiclassical* Green's functions. The material in this section is also reviewed in numerous other works, including [11] and [12] which give extensive detail. The references most closely followed here are [13], [14], [15], and [9].

3.1 The Gor'kov Equations

Because of the coherence between particles and holes in superconducting states, it is useful to work with pseudospinors in particle-hole (Nambu) space of the form $\hat{\Psi}^\dagger = (\hat{\psi}^\dagger, \hat{\psi})$, where, if spin effects are also of interest, $\hat{\psi}$ and $\hat{\psi}^\dagger$ are spinors in spin space as well. The work in this thesis, however, focusses on s-wave superconductivity in the absence of significant spin effects. Using $\hat{\Psi}^\dagger = (\psi_\uparrow^\dagger, \psi_\downarrow)$ and adding a factor of 2 to particle densities is then sufficient. The Green's function in Nambu space is given by [15]

$$\hat{G}(1,2) \equiv -i\hat{\eta}_3 \left\langle \hat{T}\Psi(1)\Psi^\dagger(2) \right\rangle \tag{3.1}$$

$$= -i\hat{\eta}_3 \begin{pmatrix} \left\langle \hat{T}\psi_\uparrow(1)\psi_\uparrow^\dagger(2) \right\rangle & \left\langle \hat{T}\psi_\uparrow(1)\psi_\downarrow(2) \right\rangle \\ \left\langle \hat{T}\psi_\downarrow^\dagger(1)\psi_\uparrow^\dagger(2) \right\rangle & \left\langle \hat{T}\psi_\downarrow^\dagger(1)\psi_\downarrow(2) \right\rangle \end{pmatrix}. \tag{3.2}$$

Transport properties can be calculated using the time dependence of $\hat{G}$

[14]. The time dependence of the field operators is given by

$$i\partial_t\psi = [\psi, \hat{H}], \tag{3.3}$$

with solutions

$$\psi(\boldsymbol{r}, t) = \exp(i\hat{H}'t)\psi(\boldsymbol{r})\exp(-i\hat{H}'t) \tag{3.4}$$

and

$$\psi^\dagger(\boldsymbol{r}, t) = \exp(i\hat{H}'t)\psi^\dagger(\boldsymbol{r})\exp(-i\hat{H}'t). \tag{3.5}$$

The field operators also obey the anticommutation relations

$$\{\psi_\alpha(\boldsymbol{r}_1), \psi^\dagger_\beta(\boldsymbol{r}_2)\} = \delta_{\alpha\beta}\delta(\boldsymbol{r}_1 - \boldsymbol{r}_2)$$

and

$$\{\psi_\alpha(\boldsymbol{r}_1), \psi_\beta(\boldsymbol{r}_2)\} = \{\psi^\dagger_\alpha(\boldsymbol{r}_1), \psi^\dagger_\beta(\boldsymbol{r}_2)\} = 0.$$

Once a suitable Hamiltonian to describe superconductivity can be determined, the time dependence of $\hat{G}$ can be found from the above properties of the field operators.

Due to the screening of the electrons' interactions with each other, one can assume that the interaction between electrons is very localised on a scale of the particle wavelength. The interaction may thus be approximated by

$$V(|\boldsymbol{r}_1 - \boldsymbol{r}_2|) = -\frac{\lambda}{2}\delta(\boldsymbol{r}_1 - \boldsymbol{r}_2),$$

where $\lambda > 0$ is the coupling constant giving the strength of the attractive interaction between electrons [2]. The non-interacting single particle energy operator is

$$\varepsilon(X) = \frac{1}{2m}\left(i\nabla_{\boldsymbol{r}} - |e|\boldsymbol{A}(X)\right)^2 - |e|V(X) - \mu,$$

where X is the set of spatial and time coordinates $(\boldsymbol{r}, t)$. In this project all applied fields are assumed to be stationary, giving a time-independent Hamiltonian. The Hamiltonian in terms of field operators, including only the local two-particle interaction (ignoring impurity scattering), takes the form

$$\hat{H} = \sum_\alpha \int \psi^\dagger_\alpha(\boldsymbol{r})\varepsilon(X)\psi_\alpha(\boldsymbol{r})d\boldsymbol{r} - \sum_{\alpha,\beta}\frac{\lambda}{2}\int \psi^\dagger_\alpha(\boldsymbol{r})\psi^\dagger_\beta(\boldsymbol{r})\psi_\beta(\boldsymbol{r})\psi_\alpha(\boldsymbol{r})d\boldsymbol{r}.$$

Using this Hamiltonian in eq. 3.3 leads to the following equations of motion for ψ_α:

$$i\partial_{t_1}\psi_\alpha(1) = [\varepsilon(\boldsymbol{r}_1) - \lambda\sum_\beta \psi^\dagger_\beta(1)\psi_\beta(1)]\psi_\alpha(1), \tag{3.6}$$

where the number 1 represents the coordinate set $(\boldsymbol{r}_1, \boldsymbol{t}_1)$. Taking the complex conjugate of eq. 3.6 gives the equation of motion for $\psi^\dagger_\alpha$ as

$$i\partial_{t_1}\psi^\dagger_\alpha(1) = \psi^\dagger_\alpha(1)[-\varepsilon(\boldsymbol{r}_1) + \lambda\sum_\beta \psi^\dagger_\beta(1)\psi_\beta(1)].$$

Acting $i\partial_{t_1}$ on each of the four Nambu Green's functions in eq. 3.1 gives 4 equations that may be grouped together into the following matrix equation known as the Gor'kov equation:

$$\begin{pmatrix}(i\partial_{t_1} - \varepsilon(1)) & \Delta(1) \\ -\Delta^*(1) & -(i\partial_{t_1} + \varepsilon^*(1))\end{pmatrix}\hat{G}(1,2) = \delta(1-2), \tag{3.7}$$

where $\Delta(1)$ is defined as

$$\Delta(1) = \lambda\langle\psi_\uparrow(1)\psi_\downarrow(1)\rangle = -i\lambda\lim_{2\to 1^-}[\hat{G}(1,2)]_{12} \tag{3.8}$$

where $[...]_{ij}$ refers to the ith row, jth column entry of the given matrix. Equation 3.8 is a self-consistent equation for Δ which is known as the superconducting order parameter. It is generally complex but its magnitude is the size of the gap in the density of states of a superconductor. In the derivation of the Gor'kov equation in eq. 3.7, several forms of 2-point Green's functions of various forms similar to $\langle\hat{T}\psi^\dagger_\alpha(1)\psi^\dagger_\beta(1)\psi_\gamma(1)\psi_\delta(2)\rangle$, are encountered. One then makes the approximation that it is roughly equal to

$$\langle\hat{T}\psi^\dagger_\alpha(1)\psi^\dagger_\beta(1)\rangle\langle\hat{T}\psi_\gamma(1)\psi_\delta(2)\rangle.$$

Contributions of the form $\langle\hat{T}\psi^\dagger\psi\rangle$ are accounted for in ε as a shift in the chemical potential, μ, and the electric potential, $V(X)$ [14].

3.2 Self-energy

Possible interactions of the particles with the material surrounding them have been neglected so far. Such interactions are usually put together into a term called the *self-energy*, denoted $\hat{\Sigma}(1,2)$. The total Green's function, including all interactions, is composed of the free particle Green's function (perhaps in the presence of applied fields), $\hat{G}_0$, plus the sum of all possible interactions at all positions and times. Written out as an equation, this appears as

$$\begin{aligned}\hat{G} &= \hat{G}_0 + \hat{G}_0\otimes\hat{\Sigma}\otimes\hat{G}_0 + \hat{G}_0\otimes\hat{\Sigma}\otimes\hat{G}_0\otimes\hat{\Sigma}\otimes\hat{G}_0 + ... \\ &= \hat{G}_0\otimes(\hat{1} + \hat{\Sigma}\otimes(\hat{G}_0 + \hat{G}_0\otimes\hat{G}_0 + ...)) \\ &= \hat{G}_0\otimes(\hat{1} + \hat{\Sigma}\otimes\hat{G}) \\ &= \hat{G}_0 + \hat{G}_0\otimes\hat{\Sigma}\otimes\hat{G},\end{aligned} \tag{3.9}$$

where $\otimes$ implies integration over common space and time coordinates as well as matrix multiplication. Equation 3.9 is a Dyson Equation. Solving for $\hat{\Sigma}$ shows that the self-energy is a functional of the full Green's function $\hat{\Sigma} = \hat{G}_0^{-1} - \hat{G}^{-1}$. Further, it is useful to note that the equation can equivalently be written

$$\hat{G} = \hat{G}_0 + \hat{G} \otimes \hat{\Sigma} \otimes \hat{G}_0, \tag{3.10}$$

which is referred to as the right-hand or conjugate Dyson equation.

The free particle Green's function was encountered implicitly in section 3.1 in its inverse form:

$$\hat{G}_0^{-1}(1,1') = (i\partial_{t_1}\hat{\eta}_3 - \hat{\varepsilon}(1))\delta(1-1'),$$

where $\hat{\varepsilon}(X) = \frac{1}{2m}\left(i\nabla_{\boldsymbol{r}} - |e|\boldsymbol{A}(X)\hat{\eta}_3\right)^2 - |e|V(X) - \mu$. The symbol $\hat{\eta}_i$ here is a Pauli-type matrix acting in Nambu space defined by

$$\hat{\eta}_1 = \begin{pmatrix} 0 & 1 \\ 1 & 0 \end{pmatrix};\ \hat{\eta}_2 = \begin{pmatrix} 0 & -i \\ i & 0 \end{pmatrix};\ \hat{\eta}_3 = \begin{pmatrix} 1 & 0 \\ 0 & -1 \end{pmatrix};$$

with similar matrices being defined for σ_i and τ_i acting in spin and Keldysh space, respectively. The free particle Green's function obeys thus [15]

$$\hat{G}_0^{-1}(1,1') \otimes \hat{G}_0(1',2) = \delta(1-2).$$

Acting $\hat{G}_{01}^{-1}(1,1') \otimes \hat{G}_0(1',2) = \delta(1-2)$ from the left on the left-hand Dyson equation in 3.9 and extracting from $\hat{\Sigma}$ the order parameter Δ produces the Gor'kov equation in eq. 3.7 but with the addition of the self-energy [13]:

$$(\hat{G}_0^{-1} + \hat{\Delta} - \hat{\Sigma})(1,1') \otimes \hat{G}(1',2) = \delta(1-2), \tag{3.11}$$

where

$$\hat{\Delta}(1,1') = \begin{pmatrix} 0 & \Delta(1) \\ -\Delta^*(1) & 0 \end{pmatrix} \delta(1-1').$$

3.3 Mixed Representations

For systems with certain symmetries, switching from the particles' respective coordinates $(\boldsymbol{r}_1, t_1)$ and $(\boldsymbol{r}_2, t_2)$ to central and relative coordinates,

$$\begin{aligned} \boldsymbol{R} &= \frac{\boldsymbol{r}_1 + \boldsymbol{r}_2}{2} \quad ; \quad \boldsymbol{r} = \boldsymbol{r}_1 - \boldsymbol{r}_2; \\ T &= \frac{t_1 + t_2}{2} \quad ; \quad t = t_1 - t_2, \end{aligned} \tag{3.12}$$

is useful. In a translationally homogeneous system, for instance, only the relative positions of the particles, $\boldsymbol{r}$, are relevant. As another example, systems with time-independent fields depend only on the relative time coordinates.

Since switching between coordinate systems in this manner is done quite frequently, some useful relations are presented here for quick reference. Only equations for position coordinates are given. The time coordinates' relations are all identical.

Firstly, the inverse relations are

$$\begin{aligned} \boldsymbol{r}_1 &= \boldsymbol{R} + \boldsymbol{r}/2 \\ \boldsymbol{r}_2 &= \boldsymbol{R} - \boldsymbol{r}/2. \end{aligned} \tag{3.13}$$

Secondly, consider the gradient operator for $\boldsymbol{R}$-space, $\nabla_{\boldsymbol{R}}$, acting on a function $f(\boldsymbol{r}_1, \boldsymbol{r}_2)$:

$$\begin{aligned} \nabla_{\boldsymbol{R}} f(\boldsymbol{r}_1, \boldsymbol{r}_2) &= \frac{\partial f}{\partial \boldsymbol{r}_1}\left(\frac{\partial \boldsymbol{r}_1}{\partial \boldsymbol{R}} = 1\right) + \frac{\partial f}{\partial \boldsymbol{r}_2}\left(\frac{\partial \boldsymbol{r}_2}{\partial \boldsymbol{R}} = 1\right) \\ &= \left(\frac{\partial}{\partial \boldsymbol{r}_1} + \frac{\partial}{\partial \boldsymbol{r}_2}\right) f; \end{aligned} \tag{3.14}$$

$$\text{so that } \nabla_{\boldsymbol{R}} = \left(\frac{\partial}{\partial \boldsymbol{r}_1} + \frac{\partial}{\partial \boldsymbol{r}_2}\right) = \nabla_{\boldsymbol{r}_1} + \nabla_{\boldsymbol{r}_2}. \tag{3.15}$$

One shows similarly that

$$\nabla_{\boldsymbol{r}} = \frac{1}{2}(\nabla_{\boldsymbol{r}_1} - \nabla_{\boldsymbol{r}_2}),$$

and

$$\nabla_{\boldsymbol{r}_1, \boldsymbol{r}_2} = \frac{1}{2}\nabla_{\boldsymbol{R}} \pm \nabla_{\boldsymbol{r}}. \tag{3.16}$$

After switching to relative/central coordinates,

$$\hat{G}(1,2) \to \hat{G}(\boldsymbol{R} + \boldsymbol{r}/2, \boldsymbol{R} - \boldsymbol{r}/2, T + t/2, T - t/2),$$

the Green's functions are often written as Fourier transforms with respect to $\boldsymbol{r}$ or ϵ or both. For the case of transforming both coordinates,

$$\hat{G}(\boldsymbol{R}, \boldsymbol{r}, T, t) = \int e^{-i\epsilon t} e^{i\boldsymbol{p}\cdot\boldsymbol{r}}\ \hat{G}(\boldsymbol{R}, \boldsymbol{p}, T, \epsilon) d\boldsymbol{p} d\epsilon. \tag{3.17}$$

Green's functions written in this form are said to be in the mixed or Wigner representations. Clearly, $i\partial_t$ and $-i\nabla_{\boldsymbol{r}}$ acting on $G(\boldsymbol{R}, \boldsymbol{r}, T, t)$ give

$$i\partial_t \to \epsilon \ \ ; \ \ -i\nabla_{\boldsymbol{r}} \to \boldsymbol{p}.$$

3.4 Matsubara Technique

The approach thus far is sufficient to consider systems at thermal equilibrium. When solving the Gor'kov equation as in eq. 3.7, e.g. for a bulk superconductor, however, poles in the Green's functions that are at a branch

cut on the real axis are encountered. How to treat these poles around the branch cut has not been addressed so far. This problem is remedied by adding an infinitesimal imaginary part to the energy which corresponds to using a retarded or advanced Green's function, as will be seen when extending to the Keldysh technique for systems out of equilibrium. At this point, however, let us consider the case of equilibrium more closely, turning to the Matsubara technique.

For a system in thermodynamic equilibrium, switching from the Green's functions described in section 3.1 to so-called temperature, or Matsubara, Green's functions proves to be useful. Matsubara Green's functions are often mathematically simpler and numerically faster than other techniques, including the Keldysh technique seen later.

The derivation of the Gor'kov equation in the Matsubara formalism is similar to that in section 3.1 with a few significant differences. The main difference is that real-time t is exchanged for imaginary time $\tau = it$. This affects the field operators $\psi(\boldsymbol{r}, t)$ and $\psi^\dagger(\boldsymbol{r}, t)$. From eqs. 3.4 and 3.5, they are replaced by

$$\psi(\boldsymbol{r}, \tau) = \exp(\hat{H}'\tau)\psi(\boldsymbol{r})\exp(-\hat{H}'\tau)$$

and

$$\psi^+(\boldsymbol{r}, \tau) = \exp(\hat{H}'\tau)\psi^\dagger(\boldsymbol{r})\exp(-\hat{H}'\tau),$$

noting that $\psi^+(\boldsymbol{r}, \tau) = \psi^\dagger(\boldsymbol{r}, -\tau)$.

The Matsubara Green's functions are defined as

$$\hat{\mathcal{G}}^M(1,2) = -\hat{\eta}_3\langle\hat{T}_\tau\hat{\Psi}(\boldsymbol{r}_1,\tau_1)\hat{\Psi}^+(\boldsymbol{r}_2,\tau_2)\rangle, \tag{3.18}$$

where $\hat{T}_\tau$ is the same as $\hat{T}$ except orders the field operators from right to left in order of increasing imaginary time τ. Averaging an operator $\hat{O}$ over the grand canonical distribution is denoted $\langle\hat{O}\rangle$:

$$\langle\hat{O}\rangle = \mathrm{Tr}\left\{\exp\left(\frac{\Omega - H'}{T}\right)\hat{O}\right\}. \tag{3.19}$$

Writing out the Green's functions in eq. 3.18 using the expression in eq. 3.19, one can use the cyclic property of the trace to show that the Matsubara Green's functions depend only on the difference $\tau = \tau_1 - \tau_2$ and are periodic in $\beta = 1/T$ according to

$$\hat{\mathcal{G}}^M(\boldsymbol{r}, -\tau) = -\hat{\mathcal{G}}^M(\boldsymbol{r}, \tau + \beta). \tag{3.20}$$

Considering Matsubara Green's functions only within $0 \leq \tau \leq \beta$ is therefore sufficient since they can be found for all other τ by eq. 3.20. This periodicity allows a Fourier series expansion of the Green's functions of the form

$$\hat{\mathcal{G}}^M(\boldsymbol{r}_1, \boldsymbol{r}_2, \tau) = T\sum_{n=-\infty}^{\infty} e^{-i\zeta_n\tau}\hat{\mathcal{G}}^M(\boldsymbol{r}_1, \boldsymbol{r}_2, \zeta_n),$$

where $\zeta_n = (2n+1)\pi T, n = 0, \pm 1, \pm 2, ...$ which are known as the Matsubara frequencies.

The real-time Gor'kov equation in eq. 3.11 rewritten for Matsubara Green's functions takes the form

$$(\hat{\mathcal{G}}_0^M + \hat{\Delta} - \hat{\Sigma})(1, 1') \otimes \hat{\mathcal{G}}^M(1', 2) = \delta(1 - 2), \tag{3.21}$$

where $\hat{\mathcal{G}}_0^M(1, 1') = (-\partial_{\tau_1}\hat{\eta}_3 - \hat{\varepsilon}(\boldsymbol{r}_1, \tau_1))$. The order parameter Δ in terms of the Matsubara Green's function retains a similar form

$$\Delta(1) = \lambda\langle\psi_\uparrow(1)\psi_\downarrow(1)\rangle = -\lambda \lim_{2\to 1^-} \hat{[}\mathcal{G}(1, 2)]_{12}. \tag{3.22}$$

Although $\psi^+(\boldsymbol{r}, \tau) = \psi^\dagger(\boldsymbol{r}, -\tau)$, the complex conjugate, Δ^*, is still the complex conjugate of Δ because of the limit $\tau \to 0$ in the definition:

$$\Delta^*(1) = \lambda\langle\psi_\downarrow^+(1)\psi_\uparrow^+(1)\rangle = -\lambda \lim_{2\to 1^-} [\hat{\mathcal{G}}(1, 2)]_{21}.$$

3.4.1 Matsubara solution for bulk superconductor

The solution of the Gor'kov equation in eq. 3.21 for a bulk superconductor in thermal equilibrium without scattering or applied fields can now be computed. The system is translationally homogeneous and also time-independent thereby promoting Fourier transformation with respect to both $\boldsymbol{r}$ and τ. For Matsubara Green's functions, this implies writing

$$\hat{\mathcal{G}}^M(\boldsymbol{r}, \tau) = T \sum_{n=-\infty}^{\infty} e^{-i\zeta_n\tau} \int e^{i\boldsymbol{p}\cdot\boldsymbol{r}} \hat{\mathcal{G}}^M(\boldsymbol{p}, \epsilon_n) d\boldsymbol{p}.$$

Substituting $\partial_{t_1} \to -i\zeta_n$ and $\varepsilon(1) \to \xi_p$ where $\xi_p \equiv p^2/2m - \mu$ and performing the inverse transforms of the resulting Gor'kov equation gives the matrix equation

$$\left(i\zeta_n - \xi_p + \hat{\Delta}\right) \hat{\mathcal{G}}^M(\boldsymbol{p}, \zeta_n) = \hat{1}. \tag{3.23}$$

Inverting eq. 3.23 gives $\hat{\mathcal{G}}^M$ as

$$\hat{\mathcal{G}}^M = \frac{1}{\xi_p^2 - E_n^2} \begin{pmatrix} -i\zeta_n - \xi_p & -\Delta \\ \Delta^* & i\zeta_n - \xi_p, \end{pmatrix}, \tag{3.24}$$

where $E_n = i\sqrt{|\Delta|^2 + \zeta_n^2}$. The Green's function has poles at $\xi_p = \pm E_n$, which, since $\xi_p \propto \nabla_{\boldsymbol{r}}$, correspond to a strong dependence of the Green's function on $\boldsymbol{r}_1 - \boldsymbol{r}_2$. These oscillations are not often of interest. The Green's function can be simplified by averaging over energies, which corresponds to integrating over ξ_p. The terms with ξ_p in the numerator are odd and so integrate to zero. For the remaining terms, the integration over ξ_p can be done using complex contour integration. This involves considering a positively oriented contour enclosing one of the poles. Since E_n is purely imaginary, all of

the poles are imaginary. For the pole at $\xi_p = E_n$, Cauchy's residue theorem gives that the integral $\int 1/(\xi_p^2 - E_n^2) d\xi_p$ evaluates to $2\pi i \mathrm{Res}(E_n) = \pi i / E_n$. The resulting Green's function is

$$\hat{\mathcal{G}}^M = \frac{1}{E_n} \begin{pmatrix} i\zeta_n & \Delta \\ -\Delta^* & -i\zeta_n \end{pmatrix}, \tag{3.25}$$

where a factor i/π was added for comparison with results presented later. The Green's function resulting from the integration $i/\pi \int \hat{\mathcal{G}}^M d\xi_p$ is known as the quasi-classical Green's function. This is discussed more later. The result in eq. 3.25 often serves as a boundary condition for calculations involving superconducting reservoirs. It is used frequently throughout this project.

The density of states can be found from eq. 3.25 by analytic continuation via

$$\nu(\epsilon) = \frac{1}{2} \mathrm{Tr}[\hat{\eta}_3 \, \hat{\mathcal{G}}^M(\zeta_n \to i\epsilon + 0)].$$

It is plotted in figure 3.1.

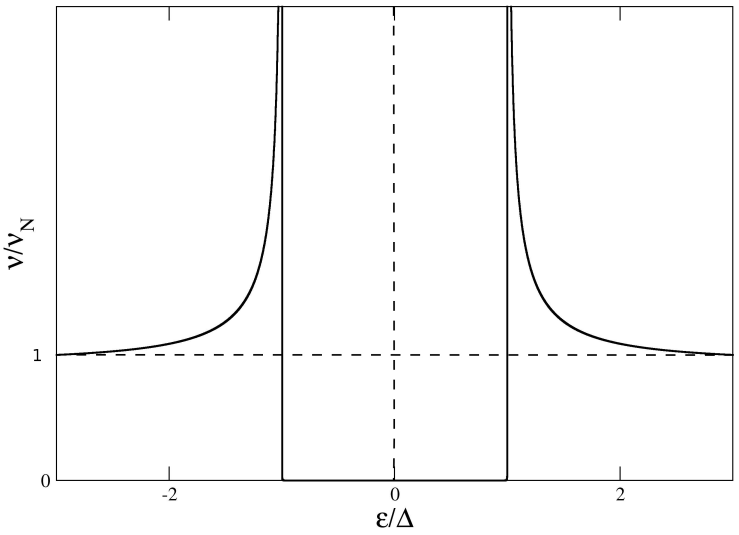

Figure 3.1: Density of states of a bulk superconductor showing the gap of width $2|\Delta|$ that opens around the Fermi energy.

3.4.2 Self-consistent gap equation

The order parameter, Δ, is given in eq. 3.22 in terms of the Green's function $[\hat{\mathcal{G}}^M]_{12}$ which in turn depends on Δ, as can be seen directly in eq. 3.24. This is what is meant by *self-consistency*. In the mixed representation

$$\begin{aligned}\Delta(\boldsymbol{r}\to 0^+,\tau\to 0^+) &= -\lambda T\sum_{n=-\infty}^{\infty}\int [\hat{\mathcal{G}}^M]_{12}(\boldsymbol{R},\boldsymbol{p},\zeta_n)d\boldsymbol{p}\\ &= -\lambda\nu_F T\sum_{n=-\infty}^{\infty}\int \frac{d\hat{\boldsymbol{p}}}{4\pi}\,[\hat{\mathcal{G}}^M]_{12}(\boldsymbol{R},\boldsymbol{p},\zeta_n)d\xi_p\\ &= -\lambda\nu_F T\sum_{n=-\infty}^{\infty}\int \langle[\hat{\mathcal{G}}^M]_{12}(\boldsymbol{R},\boldsymbol{p},\zeta_n)\rangle d\xi_p\\ &= i\pi\lambda\nu_F T\sum_{n=-\infty}^{\infty}\langle[\hat{\mathcal{G}}^M]_{12}(\boldsymbol{R},\hat{\boldsymbol{p}},\zeta_n)\rangle, \qquad (3.26)\end{aligned}$$

where $\langle ...\rangle$ denotes averaging over, $\hat{\boldsymbol{p}}$, the directions of $\boldsymbol{p}$, and $\hat{\mathcal{G}}^M(\boldsymbol{R},\hat{\boldsymbol{p}},\zeta_n) = i/\pi\int\hat{\mathcal{G}}(\boldsymbol{R},\boldsymbol{p},\zeta_n)d\xi_p$ is the quasiclassical Matsubara Green's function.

The solution for a bulk superconductor in eq. 3.25 does not depend on the direction of $\boldsymbol{p}$ so it averages to itself. The self-consistency equation 3.26 can then be solved for Δ. Using the $[\hat{g}^M]_{12}$ component of eq. 3.25 gives

$$\Delta = \lambda\nu_F\pi T\sum_{n=-\infty}^{\infty}\frac{\Delta}{\sqrt{|\Delta|^2+\zeta_n^2}}. \qquad (3.27)$$

In order to compute this sum, a cutoff energy, n_c, must be introduced because the sum is otherwise divergent. First considering the case as $T\to T_c$ so that $\Delta\to 0$, eq. 3.27 becomes

$$1 = \lambda\nu_F\sum_{n=0}^{n_c}\frac{1}{n+\frac{1}{2}},$$

where $\zeta_n = (2n+1)\pi T$ was substituted. Treating the sum as an integral and estimating that the cutoff is proportional to the inverse of the critical temperature, $n_c = a/T_c \gg 1$, then the critical temperature is

$$T_c = a\exp\left(\frac{-1}{\lambda\nu_F}\right).$$

The constant of proportionality, a, is usually said to be related to the Debye energy at which there are no phonons to mediate the attractive electron-electron interaction. Rearranging some terms and performing a similar approximation of a sum over Matsubara frequencies gives

$$\Delta\ln\left(\frac{T}{T_c}\right) = 2\pi T\sum_{n=0}^{n_c}\left(\frac{\Delta}{\sqrt{|\Delta|^2+\zeta_n^2}}-\frac{\Delta}{|\zeta_n|}\right),$$

which is the BCS gap equation for a bulk superconductor.

In cases where the approximation made here to find T_c is reasonable for non-bulk superconductors, then Δ can be computed self-consistently according to

$$\Delta = \frac{i\pi T \sum_{n=-n_c}^{n_c} \langle [\hat{\mathcal{G}}^M]_{12}(\boldsymbol{R}, \hat{\boldsymbol{p}}, \zeta_n)\rangle}{\ln\left(\frac{T}{T_c}\right) + \sum_{n=0}^{n_c} \frac{1}{|\zeta_n|}}. \tag{3.28}$$

3.5 Keldysh Green's Functions

In order to deal with problems out of thermal equilibrium, with for instance a heat gradient or an applied voltage, the Matsubara technique becomes cumbersome. For such non-equilibrium problems, another method, the Keldysh method, is advantageous. The method is based on perturbation techniques. The perturbation expansions require correct time-ordering along time-contours. The definition of the Green's function in Nambu space given in eq. 3.1 is the Green's function for the case where both time coordinates t_1 and t_2 are along the forward-in-time contour. Let this sort of time-ordered Green's function be labelled $\check{G}^{\alpha\alpha}(1,2)$, where α labels the forward-in-time contour, whereas β labels the backward-in-time contour. Other useful Green's function definitions are the following [13]:

$$\begin{aligned}
\hat{G}^{\beta\beta}(1,2) &= -i\hat{\eta}_3\langle \tilde{T}\hat{\Psi}(1)\hat{\Psi}^\dagger(2)\rangle; \\
\hat{G}^{\alpha\beta}(1,2) &= i\hat{\eta}_3\langle \hat{\Psi}^\dagger(2)\hat{\Psi}(1)\rangle; \\
\hat{G}^{\beta\alpha}(1,2) &= -i\hat{\eta}_3\langle \hat{\Psi}(1)\hat{\Psi}^\dagger(2)\rangle,
\end{aligned} \tag{3.29}$$

where $\check{G}^{\beta\beta}$ has both t_1 and t_2 on the backward-in-time contour ordered in reverse-time order. The operator $\tilde{T}$ is the reverse time-ordering operator. The functions $\check{G}^{\alpha\beta}$ and $\check{G}^{\beta\alpha}$ are recognised as the "greater-than" and "less-than" Green's functions, $\check{G}^{>}$ and $\check{G}^{<}$. Each of the matrices defined in eq. 3.29 are themselves matrices in Nambu space. They are not all linearly independent but are related by

$$\hat{G}^{\alpha\alpha}(1,2) + \hat{G}^{\beta\beta}(1,2) = \hat{G}^{\alpha\beta}(1,2) + \hat{G}^{\beta\alpha}(1,2).$$

Using eq. 3.29, the full matrix Green's function written in Keldysh space has the form

$$\check{G}(1,2) = \begin{pmatrix} \hat{G}^{\alpha\alpha}(1,2) & \hat{G}^{\alpha\beta}(1,2) \\ \hat{G}^{\beta\alpha}(1,2) & \hat{G}^{\beta\beta}(1,2) \end{pmatrix}.$$

To exploit the linear dependence of the Green's functions, the full Green's function can be first transformed $\check{G} \to \check{\tau}_3\check{G}$ and then rotated by acting

$\check{Q} = (\check{\tau}_0 - i\check{\tau}_2)/\sqrt{(}2)$ from the left and $\check{Q}^\dagger$ from the right. The resulting Green's function has the form

$$\check{G}(1,2) = \begin{pmatrix} \hat{R}(1,2) & \hat{K}(1,2) \\ \hat{0} & \hat{A}(1,2) \end{pmatrix},$$

where $\hat{R} = \hat{G}^{\alpha\alpha} - \hat{G}^{\alpha\beta}$, $\hat{A} = \hat{G}^{\alpha\alpha} - \hat{G}^{\beta\alpha}$, $\hat{K} = G^{\alpha\alpha} + G^{\beta\beta}$ are respectively the retarded, advanced, and Keldysh Green's functions. Performing similar operations on $\check{\Sigma}$, the form of the Dyson equation for the full Green's functions including the Keldysh space is the same:

$$\check{G} = \check{G}_0 + \check{G}_0 \otimes \check{\Sigma} \otimes \check{G}.$$

Extracting the self-energy again, the Gor'kov equation including Keldysh space is also the same:

$$(\check{G}_0^{-1} + \check{\Delta} - \check{\Sigma})(1,1') \otimes \check{G}(1',2) = \delta(1-2),$$

where

$$\check{\Delta} = \begin{pmatrix} \hat{\Delta} & 0 \\ 0 & \hat{\Delta} \end{pmatrix};\ \check{G}_0^{-1} = \begin{pmatrix} \hat{G}_0^{-1} & 0 \\ 0 & \hat{G}_0^{-1} \end{pmatrix}.$$

All spectral information can be found from $\hat{R}$, which is related to $\hat{A}$ by $\hat{R}(1,2) = -\hat{\eta}_3 \hat{A}^\dagger(2,1)\hat{\eta}_3$. Information regarding occupation of states, however, is contained solely in the Keldysh Green's function $\hat{K}$.

3.6 Eilenberger Equation

At this point, simplifications can be made to adjust the detail and complexity of the Green's function theory to a level appropriate for the systems to be studied. Only stationary cases, in which all applied fields are constant in time, will be considered. This encourages switching to the central and relative time coordinates, T and t, as described in section 3.3 because only the relative time coordinate is required. Switching to relative and central position coordinates $\boldsymbol{R}$ and $\boldsymbol{r}$ will also be useful because all fields will be assumed to depend only on $\boldsymbol{R}$ and not $\boldsymbol{r}$. The mixed representation as presented in eq. 3.17 is thus used.

As seen in eq. 3.24, the Green's functions depend strongly on ε_p and ϵ. Since $\varepsilon_p \to \nabla_{\boldsymbol{r}}$, this corresponds to a strong dependence of the Green's functions on small length scales. The characteristic length scales of superconductivity, $\xi_0 = v_F/\Delta$ and $\xi_N = v_F/2\pi T$, however, are much larger than the Fermi wavelength, λ_F. Subtracting the right-hand Dyson equation, eq. 3.10, from the left-hand one, eq. 3.9, reduces this dependence on ξ_p and ϵ to weak a one [15]. This step, known as the left-right trick, allows taking

an average over energy by integrating over ξ_p, resulting in the *semiclassical* Green's function,

$$\check{G}(\boldsymbol{R}, \hat{\boldsymbol{p}}; \epsilon) = \frac{i}{\pi} \int d\xi \check{G}(\boldsymbol{R}, \boldsymbol{p}; \epsilon).$$

After transforming to the mixed representation, the convolutions, $\otimes$, in the Gor'kov equation need to be addressed. They can be expanded using a gradient expansion, i.e. rewriting convolution in the following manner:

$$A \otimes B = \int dt_3 e^{\frac{i}{2}(\nabla^A_{\boldsymbol{R}} \cdot \nabla^B_{\boldsymbol{p}} - \nabla^A_{\boldsymbol{p}} \cdot \nabla^B_{\boldsymbol{R}})} A(\boldsymbol{R}, \boldsymbol{p}, t_1, t_2) B(\boldsymbol{R}, \boldsymbol{p}, t_1, t_2).$$

Specifically, when Fourier transforming to central and relative coordinates in both position and time, the gradient expansion may be written in the following form when performing the left-right trick if there is assumed to be no dependence on central time, T [13]:

$$(A \ominus B)(\boldsymbol{R}, \boldsymbol{p}, \epsilon) = [A, B] + \frac{i}{2} \left[\{\nabla_{\boldsymbol{R}} A, \nabla_{\boldsymbol{p}} B\} - \{\nabla_{\boldsymbol{p}} A, \nabla_{\boldsymbol{R}} B\} \right].$$

As mentioned, the dependence of the Green's function on ξ_p is weak after the left-right trick. In addition, only the diffusive (dirty) limit will be considered in this work, so that the quantities involved in the Gor'kov equation have little dependence on the direction of $\boldsymbol{p}$. The gradients in $\boldsymbol{p}$ in the gradient expansion can thus be neglected. Excluding external fields, with all the simplifications mentioned above, the resulting equation for the Green's function, $\check{G}$, is

$$\frac{i}{\hbar}[\check{E}, \check{G}] + \boldsymbol{v} \cdot \nabla_{\boldsymbol{R}} \check{G} = \frac{i}{\hbar}[\check{\Sigma}, \check{G}], \tag{3.30}$$

known as the Eilenberger equation [16]. The commutators in eq. 3.30 involve only matrix multiplication. Note the change in notation. In switching to the mixed representation and considering only lowest order gradients

$$G_0^{-1} = i\partial_{t_1} + \frac{1}{2m}\nabla^2_{\boldsymbol{r}_1} + \mu \to \epsilon + \frac{i}{2m}\boldsymbol{p} \cdot \nabla_{\boldsymbol{R}} + \mu$$

by eq. 3.16. Since all transport happens around the Fermi surface, all quantities are replaced by their values there, for instance $\boldsymbol{p} \to m\boldsymbol{v}_f$. The matrix $\check{E}$ is defined by $\check{E}(\boldsymbol{R}, \epsilon) = \check{G}_0^{-1}(\boldsymbol{R}, \boldsymbol{p}, \epsilon) - \frac{i}{2m}\boldsymbol{p} \cdot \nabla_{\boldsymbol{R}} - \mu + \check{\Delta}$. Expressed instead in Nambu space it has the form

$$\check{E} \equiv \epsilon\hat{\eta}_3 + \frac{\Delta}{2}(i\hat{\eta}_2 + \hat{\eta}_1) + \frac{\Delta^*}{2}(i\hat{\eta}_2 - \hat{\eta}_1) = \begin{pmatrix} \epsilon & \Delta \\ -\Delta^* & -\epsilon \end{pmatrix}.$$

The Eilenberger equation as developed so far is insufficient to give an unique solution to any problem. Prior to performing the left-right trick, the Gor'kov equation was inhomogeneous and produced therefore a single possible solution, i.e. the equation was normalised. The left-right trick instead

produces an homogeneous equation, determing the solution up to a constant factor. The Eilenberger equation should of course give correct results so the appropriate normalisation needs to be restored. Since $\check{G}[\check{E},\check{G}]+[\check{E},\check{G}]\check{G}=0$ and $\check{G}[\check{\Sigma},\check{G}]+[\check{\Sigma},\check{G}]\check{G}=0$, the Eilenberger equation reveals that $\check{G}^2$ is independent of $\boldsymbol{R}$:

$$\nabla_{\boldsymbol{R}}\check{G}^2=\check{G}(\nabla_{\boldsymbol{R}})\check{G}+(\nabla_{\boldsymbol{R}}\check{G})\check{G}=0. \tag{3.31}$$

This means that if the Green's function of a reservoir is known, then $\check{G}^2$ is known throughout the entire structure. The solution for a superconducting reservoir was given in the Matsubara formalism in eq. 3.25 for which $\hat{\mathcal{G}}^2=\hat{1}$. The retarded Green's function in the reservoir can be obtained by analytic continuation, $\hat{R}=\hat{\mathcal{G}}(\zeta_n\to i\epsilon+0)$. Clearly then $\hat{R}^2=\hat{1}$ as well. The advanced Green's function can then be obtained by $\hat{A}=-\hat{\eta}_3\hat{R}^\dagger\hat{\eta}_3$ so $\hat{A}^2=\hat{1}$ also. Since reservoirs are assumed to be in equilibrium, the Keldysh component is found from $(\hat{R}-\hat{A})\tanh(\epsilon/2T)$ giving that $\hat{R}\hat{K}+\hat{K}\hat{A}=0$ there. The square of the full reservoir Green's function in Keldysh space is at last $\check{G}^2=\check{1}$ since $\hat{R}\hat{K}+\hat{K}\hat{A}=0$. Equation 3.31 implies then that $\hat{\mathcal{G}}^2=\hat{1}$ and $\check{G}^2=\check{1}$ everywhere in the nanostructure. By these arguments, the normalisation condition is restored. That $\check{G}^2=\check{1}$ is often useful in calculations. Some simple but useful relations are provided in the appendix section A. The normalisation condition is discussed in more detail in [17].

3.6.1 The Keldysh component and distribution functions

The $\hat{R}\hat{K}+\hat{K}\hat{A}=0$ condition is automatically fulfilled by the following parameterisation of the Keldysh component,

$$\hat{K}=\hat{R}\hat{h}-\hat{h}\hat{A}, \tag{3.32}$$

where $\hat{h}$ is a matrix containing the information about the particles' distribution. Inserting this form of the Keldysh component into the Usadel equation gives a kinetic equation of motion that is linear in $\hat{h}$ implying that it may be assumed to be diagonal [15]. This is commonly done by separating $\hat{h}$ into 'longitudinal' and 'transverse' components f_L and f_T as $\hat{h}=f_L+f_T\hat{\eta}_3$. The longitudinal component, f_L, is related to effective temperature change while the transverse f_T is related to changes in the effective chemical potential. At equilibrium these functions are

$$f_{L(T)}=\frac{1}{2}\left[\tanh\left(\frac{\epsilon+eV}{2T}\right)+(-)\tanh\left(\frac{\epsilon-eV}{2T}\right)\right]. \tag{3.33}$$

Once $\hat{R}$ and $\hat{A}$ are known, the Keldysh Green's function is found from the parameterisation given in eq. 3.32. Since the superconducting reservoirs

to be used as boundary conditions are at equilibrium and all at the same potential, $V = 0$, using eq. 3.33 gives

$$\hat{K} = (\hat{R} - \hat{A}) \tanh\left(\frac{\epsilon}{2T}\right), \tag{3.34}$$

where we know $\hat{R}$ and $\hat{A}$ from above. In the case of normal metals where $\hat{R} = -\hat{A} = \hat{\eta}_3$,

$$\hat{K} = 2 \begin{pmatrix} \tanh\left(\frac{\epsilon+eV}{2k_BT}\right) & 0 \\ 0 & -\tanh\left(\frac{\epsilon-eV}{2k_BT}\right) \end{pmatrix}.$$

3.7 Usadel Equation

Similarly to the classical case, the dirty limit allows significant simplification of the Eilenberger equation, eq. 3.30. Also as in the classical case, only elastic impurity scattering will be included, again using the Born approximation. The derivation given here again follows that given in [9] closely. As before, the scattering rate

$$W_{\boldsymbol{p},\boldsymbol{p}'} = \frac{c_{imp}}{\hbar} |\tilde{U}_{imp}(\boldsymbol{p} - \boldsymbol{p}')|^2 \delta(E(\boldsymbol{p}) - E(\boldsymbol{p}')),$$

and the relaxation time

$$\tau_P^{-1} = \frac{2\pi\nu c_{imp}}{\hbar} |\tilde{U}_{imp}|^2,$$

are used. Writing the self-energy, $\check{\Sigma}(\boldsymbol{p})$, as

$$\check{\Sigma}(\boldsymbol{p}) = \int d\boldsymbol{p}' W_{\boldsymbol{p}\boldsymbol{p}'} \check{G}(\boldsymbol{p}'),$$

and rewriting $\int d\boldsymbol{p}' \to \int\int \nu_F d\hat{\boldsymbol{p}}' d\xi_p$ gives $\check{\Sigma}$ as a functional of the quasiclassical $\check{G}$:

$$\check{\Sigma}(\boldsymbol{p}) = \frac{-i\hbar}{2\tau_p} \langle \check{G}(\hat{\boldsymbol{p}}) \rangle.$$

As in section 2.2, a first-order approximation of the Green's function consisting of an isotropic part, $\check{G}(\boldsymbol{R})$, plus a small anisotropic part, $\check{G}^{(1)}(\boldsymbol{R}, \hat{\boldsymbol{p}})$, is useful: $\check{G} \to \check{G}(\boldsymbol{R}) + \check{G}^{(1)}(\boldsymbol{R}, \hat{\boldsymbol{p}})$ with $\check{G} \gg \check{G}^{(1)}$ and $\left\langle \check{G}^{(1)} \right\rangle = 0$. Inserting this expanded $\check{G}$ into the expression for the impurity self-energy, leads to

$$\check{\Sigma} = \frac{-i\hbar}{2\tau_P} \left\langle \check{G}(\boldsymbol{R}, \hat{\boldsymbol{p}}) \right\rangle \to \frac{-i\hbar}{2\tau_P} \left\langle \check{G}(\boldsymbol{R}) + \check{G}^{(1)}(\boldsymbol{R}, \hat{\boldsymbol{p}}) \right\rangle = \frac{-i\hbar}{2\tau_P} \check{G}.$$

Now using the expanded Green's function in eq. 3.30 gives

$$\frac{i}{\hbar}[\check{E}, \check{G} + \check{G}^{(1)}] - \boldsymbol{v} \cdot \nabla_{\boldsymbol{R}} \left(\check{G} + \check{G}^{(1)}\right) = \frac{1}{2\tau_P} \left[\check{G}, \check{G} + \check{G}^{(1)}\right]. \tag{3.35}$$

This equation will provide two equations: an averaged and a non-averaged one.

Before turning to these equations, the right hand side of eq. 3.35 can be simplified by noting that $[\check{G}, \check{G} + \check{G}^{(1)}] = [\check{G}, \check{G}^{(1)}]$. Using that $\check{G} \gg \check{G}^{(1)}$ allows rewriting $\check{G}^2 = (\check{G} + \check{G}^{(1)})^2 \approx \check{G}^2 + \check{G}\check{G}^{(1)} + \check{G}^{(1)}\check{G}$. Requiring $\check{G}^2 = \check{1}$ leads to $\{\check{G}, \check{G}^{(1)}\} = \check{G}\check{G}^{(1)} + \check{G}^{(1)}\check{G} = \check{0}$, which is used to simplify in the following step.

For the non-averaged equation, using $\check{G} \gg \check{G}^{(1)}$ gives

$$\frac{i}{\hbar}[\check{E}, \check{G}] - \boldsymbol{v} \cdot \nabla_{\boldsymbol{R}} \check{G} = \frac{1}{2\tau_P} \left[\check{G}, \check{G}^{(1)}\right] = \frac{1}{\tau_P} \check{G}\check{G}^{(1)}. \tag{3.36}$$

Taking the average of eq. 3.35 over directions $\hat{\boldsymbol{p}}$ and using that $\left\langle \check{G}^{(1)} \right\rangle = 0$ gives

$$\frac{i}{\hbar}[\check{E}, \check{G}] - \nabla_{\boldsymbol{R}} \cdot \check{\boldsymbol{j}} = 0; \ \check{\boldsymbol{j}} \equiv \left\langle \boldsymbol{v} \check{G}^{(1)} \right\rangle. \tag{3.37}$$

The $\check{\boldsymbol{j}}$ is the spectral matrix current density which will be important later when discussing circuit theory. The minus sign is to emphasise the similarity between the equations to follow and the classical equations of section 2.2. The above step used that $\nabla \cdot (f\boldsymbol{A}) = (\nabla f) \cdot \boldsymbol{A} + f(\nabla \cdot \boldsymbol{A})$. This means that $\left\langle \boldsymbol{v} \cdot \nabla_{\boldsymbol{R}} \check{G}^{(1)} \right\rangle = \left\langle \nabla_{\boldsymbol{R}} \cdot (\boldsymbol{v} \check{G}^{(1)}) - (\nabla_{\boldsymbol{R}} \cdot \boldsymbol{v}) \check{G}^{(1)} \right\rangle$. Part of the assumption of isotropisation is, however, that $\nabla_{\boldsymbol{R}} \cdot \boldsymbol{v} \approx 0$. Thus

$$\left\langle \boldsymbol{v} \cdot \nabla_{\boldsymbol{R}} \check{G}^{(1)} \right\rangle = \nabla_{\boldsymbol{R}} \cdot \left\langle \boldsymbol{v} \check{G}^{(1)} \right\rangle.$$

Substracting eq. 3.37 from eq. 3.36 leads to

$$-\boldsymbol{v} \cdot \nabla_{\boldsymbol{R}} \check{G} = \frac{1}{\tau_P} \check{G}\check{G}^{(1)}.$$

which gives

$$\check{G}^{(1)} = -\tau_P \boldsymbol{v} \ \check{G} \ \nabla_{\boldsymbol{R}} \check{G}. \tag{3.38}$$

Using eq. 3.38 in eq. 3.37 gives the so-called Usadel equation for diffusive nanostructures [6]:

$$\nabla_{\boldsymbol{R}} \cdot \check{\boldsymbol{j}} - \frac{ie^2\nu}{\hbar}[\check{E}, \check{G}] = 0; \ \check{\boldsymbol{j}} = -\sigma \ \check{G} \nabla_{\boldsymbol{R}} \check{G}, \tag{3.39}$$

where a factor $e^2\nu$ was added in order to have $\check{\boldsymbol{j}}$ in units of conductivity. The Usadel equation is clearly analogous to the drift-diffusion equation from eq. 2.3. The apparent correspondance of $\check{G}\nabla_{\boldsymbol{R}}\check{G}$ to the classical ∇V explains that the Green's functions are also known as matrix voltages.

Chapter 4

Finite-element quantum circuit theory

The required background for Nazarov's quantum circuit theory [8] was introduced in chapters 2 and 3. This chapter shows how quantum circuit theory arises naturally from the semiclassical results of chapter 3 and relates it to classical circuit theory.

4.1 Classical circuit theory

For classical circuits, solving the Laplace equation (eq. 2.7), while correct, is often a needlessly complicated task. The simpler and more commonly familiar approach is instead to approximate the circuit by breaking it into different elements: terminals, nodes and connectors. Terminals are the sources of the applied voltages, where the electrons are injected into (or removed from) the rest of the circuit. Nodes are the small volume elements that form the circuit when added together. To be a node, such a volume element should have negligible potential differences across it when compared to between it and adjacent nodes. The connections between the nodes, fittingly referred to as connectors, are regions across which the potential changes significantly. They are characterised by the conductance of the material. In more familiar terms of standard circuit analysis, for instance, a connector would be a resistor connecting two good conductors (nodes).

The point is then to be able to determine the current through each of the connectors and the potential in each of the nodes, given the potentials of the terminals. This is most often accomplished using Kirchhoff's current rule and Ohm's law. Kirchoff's current rule, for clarity later on, is a current balance equation stating that the sum of all currents into and out of a node i to and from the connected nodes k is zero, i.e.

$$\sum_k I_{ik} = 0.$$

It is essentially the result of integrating the Laplace equation over a volume, $\int(\nabla \cdot \boldsymbol{I})dV = \int(\boldsymbol{N} \cdot \boldsymbol{I})dA = 0$, but where the surface integral is separated into finite elements, i.e. the connectors to the neighbouring nodes. In the finite-element picture, Ohm's law from eq. 2.7 becomes $I_{ik} = G_{ik}(V_i - V_k)$, that is, that the current through the connector between nodes i and k is given by the potential difference between the nodes and the characteristic conductance of the connector, G_{ik}. In this sense, Ohm's law acts as a boundary condition for the two ends of the connector.

4.2 Conservation equation

The classical circuit theory described in chapter 2 relied on two things: a current conservation equation (eq. 2.7) and a boundary condition (Ohm's law) for the regions of greater potential differences. Section 3 began with the Green's function methods standard to studies of superconductivity leading to the Eilenberger and Usadel equations which were clearly similar in nature to the balance equations of chapter 2. The Usadel equation particularly,

$$\nabla_{\boldsymbol{R}} \cdot \check{\boldsymbol{j}} - \frac{ie^2\nu}{\hbar}[\check{E}, \check{G}] = 0; \ \check{\boldsymbol{j}} = -\sigma \ \check{G} \ \nabla_{\boldsymbol{R}}\check{G}, \tag{4.1}$$

may be seen as a non-conservation equation, indicating that there is some "leakage" due to the $[\check{E}, \check{G}]$ term. Redefining the sum of matrix currents to include the leakage allows the Usadel equation to be considered a conservation equation instead. To do so, the volume leakage current is defined as

$$\check{j}_{lc} \equiv -\frac{ie^2\nu}{\hbar}[\check{E}, \check{G}].$$

With this and integrating eq. 4.1 over volume results in an expression for spectral current,

$$\check{I}_{tot} = \check{I} + \check{I}_{lc} = \int(\check{\boldsymbol{j}} \cdot \boldsymbol{N})dA - \int \frac{ie^2\nu}{\hbar}[\check{E}, \check{G}]dV = 0, \tag{4.2}$$

where $\boldsymbol{N}$ is a unit vector in the direction of the surface at the point of integration and dA is a surface area element. The leakage current $\check{I}_{lc} = -\int ie^2\nu[\check{E}, \check{G}]/\hbar \ dV$ has the same form as other connectors and may be seen as a ficitious terminal connected to the node.

Discretising the integrals in eq. 4.2 gives the following generalised Kirchhoff current rule for quantum circuits:

$$\sum_k \check{I}_{ik} + \check{I}_{lc} = 0. \tag{4.3}$$

This is the equation used to construct a quantum circuit theory in the same sense as is done with the drift-diffusion equation in classical circuit theory.

How to divide nanostructures into nodes will be discussed later. What remains to complete a quantum circuit theory is a boundary condition for connectors analogous to Ohm's law.

4.3 Boundary condition

Regardless of the type of connector (point contact, tunnel junction,...) between two nodes, provided that the transport within is diffusive with no inelastic scattering, then an appropriate boundary condition for the matrix current across it may be written, rather compactly, as [8]

$$\check{I}_{ik} = G_Q \sum_p \frac{T_p[\check{G}_i, \check{G}_k]}{2 + (T_p/2)(\{\check{G}_i, \check{G}_k\} - 2)}, \tag{4.4}$$

where the T_p are the set of transmission eigenvalues of the scattering matrix specific to each kind of junction. Tunnel junctions, for instance, have only small transmission eigenvalues, $T_p \to 0$, leading to the Kuprianov-Lukichev boundary condition [18]

$$\check{I}_{ik} = \frac{G_T}{2}[\check{G}_i, \check{G}_k], \tag{4.5}$$

where $G_T = G_Q \sum_p T_p$ and $G_Q = 2e^2/h$ is the conductance quantum. Equation 4.4 concisely contains a lot of information about Josephson junctions, much of which can be derived derictly from it. See the end of appendix section E for an example derivation.

Equation 4.4 can be written in another form in terms of the "matrix phase" $\check{\phi} \equiv -i \ln(\check{G}_1 \check{G}_2)$ as [9]

$$\check{I} = i\mathcal{I}(\check{\phi}); \quad \mathcal{I}(\phi) = G_Q \sum_p \frac{T_p \sin\phi}{1 - T_p \sin^2(\phi/2)}. \tag{4.6}$$

See appendix section D for a derivation. This form can be used to gain insight into the relation between transmission distribution functions, $\rho(T)$, and the matrix structure.

4.4 Separation of a nanostructure into elements

With a conservation equation and a boundary condition established, the finite-element circuit theory is completed. The first thing to consider then is how to divide a nanostructure into elements. Put simply, a region where the matrix voltage, the Green's function $\check{G}$, changes rapidly is regarded as a connector, whereas regions where it is relatively constant can be regarded as nodes. Given that all circuits considered here include superconductors, a natural upper limit on the size of nodes is the coherence length, given by $\xi_0 = \sqrt{\hbar D/(2\max(\Delta, \epsilon))}$. Increasing the number of nodes/divisions should

increase accuracy. A real nanostructure is typically already divided into separate elements that should give insight as to how to divide it for calculations.

The example of dividing a bulk diffusive conductor is illustrative [8]. The volume of the conductor is divided into a mesh of cubic nodes with sides of length a, separated exclusively by tunnel junction connectors. Equation 4.5 can then be used. The period a should be small enough to simulate continuous conductivity throughout the conductor. Practically speaking, one wishes of course for as large a's as possible to have as few nodes to compute as possible while retaining the desired accuracy.

Consider a node i centered at point $\boldsymbol{r}_i$, having volume $V_i = a^3$. Given that the condition for a volume to be considered a node is that its Green's function vary little in space, approximate the Green's function of node i by

$$\check{G}_i(\boldsymbol{r}) = \check{G}(\boldsymbol{r}_i) + \check{\boldsymbol{\Xi}} \cdot (\boldsymbol{r} - \boldsymbol{r}_i), \tag{4.7}$$

similarly to as was done in section 3.7, where $a\boldsymbol{\Xi} \ll \check{G}(\boldsymbol{r}_i)$. Using eq. 4.7 in $\check{\boldsymbol{j}} = -\sigma\check{G}\nabla\check{G}$ from section 3.7,

$$\check{\boldsymbol{j}} = -\sigma\check{G}(\boldsymbol{r}_i)\check{\boldsymbol{\Xi}}. \tag{4.8}$$

Recalling that the total current is given by $\check{I} = \int(\check{\boldsymbol{j}} \cdot \boldsymbol{N})dA$, the current flowing into node i through the surface connecting node k is

$$\check{I}_{ik} = A\check{j}_{ik}, \tag{4.9}$$

where $A = a^2$ is the surface area of the connector and $\check{j}_{ik}$ is the component of the matrix current density in the direction from node k towards node i, $\check{\boldsymbol{j}} \cdot \boldsymbol{N}_{ik}$. Note that N_{ik} points in towards the node i.

Now let us apply the boundary condition eq. 4.5 and write the Green's function of node i as above and that of node k as $\check{G}_k = \check{G}(\boldsymbol{r}_i) + \check{\boldsymbol{\Xi}} \cdot (\boldsymbol{r} - \boldsymbol{r}_i - l\boldsymbol{N}_{ik})$, where $l = a$ is the distance between the centers of the nodes, written as l to distinguish it from the surface area of the connector. Clearly then $\check{G}_k = \check{G}_i + \check{\boldsymbol{\Xi}} l\boldsymbol{N}_{ik}$ giving

$$\check{I}_{ik} = \frac{G_T}{2}[\check{G}(\boldsymbol{r}_i), \check{\boldsymbol{\Xi}} \cdot (-l\boldsymbol{N}_k)] = -G_T l\ \check{G}(\boldsymbol{r}_i)\check{\Xi}_k, \tag{4.10}$$

which indeed reproduces eq. 4.8. Comparing eqs. 4.10 and 4.9, shows that $\sigma = G_T l/A$ or, using conductance per unit area, $g_T \equiv G_T/A = \sigma/l$.

As mentioned, to increase accuracy, the nodes composing a structure can be made smaller. This implies imagining the presence of connectors in regions of the structure where there may not actually exist any such connector. This point, which may seem confusing, is addressed later in section 5.2.1.

4.5 Applying the finite-element circuit theory

In this section, an algorithm for computing the Green's functions in the nodes as given in [8] is described. The algorithm was the basis for most of the calculations performed in this thesis project.

The boundary condition eq. 4.4 can always be written as $\check{I}_{ik} = [\check{G}_i, \check{L}_{ik}]$ where $\check{L}$ is a matrix. This allows the Kirchhoff's current rule eq. 4.3 to be written as

$$[\check{G}_i, \check{\mathcal{G}}_i] = 0, \tag{4.11}$$

where

$$\check{\mathcal{G}}_i = \sum_k \check{L}_{ik} - \frac{ie^2\nu V_i}{\hbar}\check{E},$$

where $\check{L}_{ik}$ generally depends on $\check{G}_i$.

Writing

$$\check{\mathcal{G}} = \begin{pmatrix} \hat{\mathcal{R}} & \hat{\mathcal{K}} \\ 0 & \hat{\mathcal{A}} \end{pmatrix}$$

and inserting it into eq. 4.11 produces the following relations: $[\hat{R}, \hat{\mathcal{R}}] = 0$, $[\hat{A}, \hat{\mathcal{A}}] = 0$ and $\hat{R}\hat{\mathcal{K}} + \hat{K}\hat{\mathcal{A}} = \hat{\mathcal{R}}\hat{K} + \hat{\mathcal{K}}\hat{A}$. The first two imply that

$$\hat{R} = \hat{\mathcal{R}}/\boldsymbol{r}\ ; \quad \hat{A} = \hat{\mathcal{A}}/\boldsymbol{a},$$

where $\boldsymbol{r}$ and $\boldsymbol{a}$ are just normalisation constants. Using these expressions together in $\hat{R}^2, \hat{A}^2 = \hat{1}$ gives

$$\boldsymbol{r} = \sqrt{\frac{\mathrm{Tr}(\hat{\mathcal{R}}^2)}{2}}\ ; \quad \boldsymbol{a} = \sqrt{\frac{\mathrm{Tr}(\hat{\mathcal{A}}^2)}{2}}.$$

The symmetry relation $\hat{A} = -\hat{\eta}_3\hat{R}^\dagger\hat{\eta}_3$ may then be used to show that

$$\boldsymbol{a} = \boldsymbol{r}^*.$$

The Keldysh part is found by left-multiplying the equation $\hat{R}\hat{\mathcal{K}} + \hat{K}\hat{\mathcal{A}} = \hat{\mathcal{R}}\hat{K} + \hat{\mathcal{K}}\hat{A}$ by $\hat{R}$ and using that $\hat{R}^2, \hat{A}^2 = \hat{1}$ and $\hat{R}\hat{K} = -\hat{K}\hat{A}$, giving

$$\hat{K} = \frac{1}{\boldsymbol{a} + \boldsymbol{r}}(\hat{\mathcal{K}} - \hat{R}\hat{\mathcal{K}}\hat{A}).$$

We now have equations for the conservation of current in the nodes in terms of the connected nodes. To approach a circuit consisting of several nodes and connectors, the conservation equation can be applied in each of the nodes to determine the Green's functions. Given that the Green's functions of the reservoirs are known, inserting estimated Green's functions for the nodes in the conservation equations and iterating will determine the

Green's functions in the nodes. Once the Green's functions in all of the nodes are found, any transport quantity can be deduced. The density of states may be found from

$$\frac{\nu(\epsilon)}{\nu} = \frac{1}{2}\,\mathrm{Re}[\mathrm{Tr}(\hat{\eta}_3\hat{R})]. \tag{4.12}$$

The electric current between node i and node k is found from the Keldysh component of the matrix current by

$$I_{ik} = \frac{1}{4e}\int \mathrm{Tr}(\hat{\eta}_3\hat{I}^K_{ik})d\epsilon. \tag{4.13}$$

The expression for current in the Matsubara technique is instead

$$I_{ik} = -\,\mathrm{Im}\left[\frac{\pi}{2e}T\sum_{\zeta}\mathrm{Tr}(\hat{\eta}_3\hat{I}_M)\right].$$

Chapter 5

Application to Josephson Junctions

In this chapter, transport through diffusive SNS and SS'S type Josephson junctions (see [19] and [20] for reviews) is calculated using the quantum circuit theory. All connectors were considered to be tunnel junctions. In this work two different SNS type scenarios were considered. The first scenario, discussed in section 5.1, was an STNTS junction where the tunnel junctions' resistances are much greater than the resistance of the intermediate N metal. The second SNS scenario was to model a short, diffusive, normal wire between two superconducting reservoirs. This case was derived analytically from the Usadel equation by Kulik and Omel'yanchuk (KO1) [10]. Section 5.2 discusses the scenario and why the nodecode for tunnel junctions is able to model this system which contains no tunnel junctions. The KO1 current equation is also derived in section 5.2.2.

Additional care must be taken when the nodes of the circuit theory are superconducting. Section 5.3 identifies some challenges that are encountered in these cases as well as describes how to resolve them.

Note that in the following calculations, a dimensionless parameter, g, is used to characterise the junctions. It is given by

$$g \equiv \frac{2\pi G_T}{1.76\sigma_N A}\left(\frac{\xi_N^2}{L}\right),$$

where σ_N is the normal state conductivity of the intermediate material, A is the cross-sectional area of the nodes, L is the length of the junction between the reservoirs, and ξ_N is the coherence length of the normal metal given by $\xi_N^2 = \frac{1.76}{2\pi}\frac{\hbar D}{\Delta_0}$ with $\Delta_0 = 1.76kT_c$ where T_c is the critical temperature of the reservoirs. The parameter g is related to the leakage current prefactor $e^2\nu_F V_N/\hbar$ by

$$G_T/g = e^2\nu_F V_N/\hbar.$$

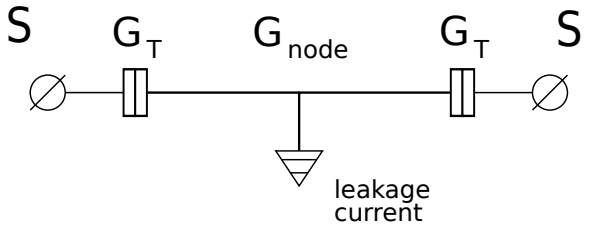

Figure 5.1: The circuit diagram after discretising the STNTS junction, assuming that the tunnel junction resistances are much greater than the resistance of the intermediate normal metal, $R_T \gg R_N$, and that the length of the normal metal is much shorter than the coherence length in the normal metal, $\xi_N \gg L$.

5.1 STNTS

All connectors are assumend to be tunnel junctions making eq. 4.5,

$$\check{I}_{i,k} = \frac{G_T}{2}[\check{G}_i, \check{G}_k],$$

applicable for the connectors. This simplifies the expression for $\check{\mathcal{G}}_i$ to be independent of $\check{G}_i$:

$$\check{\mathcal{G}}_i = \frac{G_{T,i-1}}{2}\check{G}_{i-1} + \frac{G_{T,i}}{2}\check{G}_{i+1} - i\frac{e^2\nu}{\hbar}V_i\check{E}.$$

By the assumption that all superconductors are at voltage $V = 0$ and that there are no temperature gradients, the system is at equilibrium and so only the retarded Green's function $\hat{R}_i$ needs to be determined.

Assuming that the tunnel junctions' resistances, R_T, are much larger than the resistance of the N metal, R_N, and that the length of the N metal, L, is much shorter than the coherence length, ξ_N, the intermediate metal may be treated as a single node. More specifically, the second condition should be $(L/\xi_N)^2 \ll R_N/\epsilon$. To see this, consider the equations if one divides the intermediate metal into two nodes. The equation for the first node is then

$$\hat{\mathcal{R}}_1 = \frac{1}{2R_T}\hat{R}_L + \frac{1}{2R_N}\hat{R}_2 - i\frac{1.76}{2\pi}\left(\frac{L/2}{\xi_N}\right)^2\frac{\epsilon}{R_N}\hat{\eta}_3.$$

The assumptions that $R_T \gg R_N$ and $\xi_N \gg L$ reduce the equation to simply

$$\hat{\mathcal{R}}_1 \approx \frac{1}{2R_N}\hat{R}_2,$$

which gives in turn $\hat{R}_1 \approx \hat{R}_2$ since $\boldsymbol{r} = \sqrt{\mathrm{Tr}(\mathcal{R}_1^2)/2} \approx G_N/2$. Because the Green's functions in the nodes are roughly equal, calculating for more than a single node does not provide much additional information.

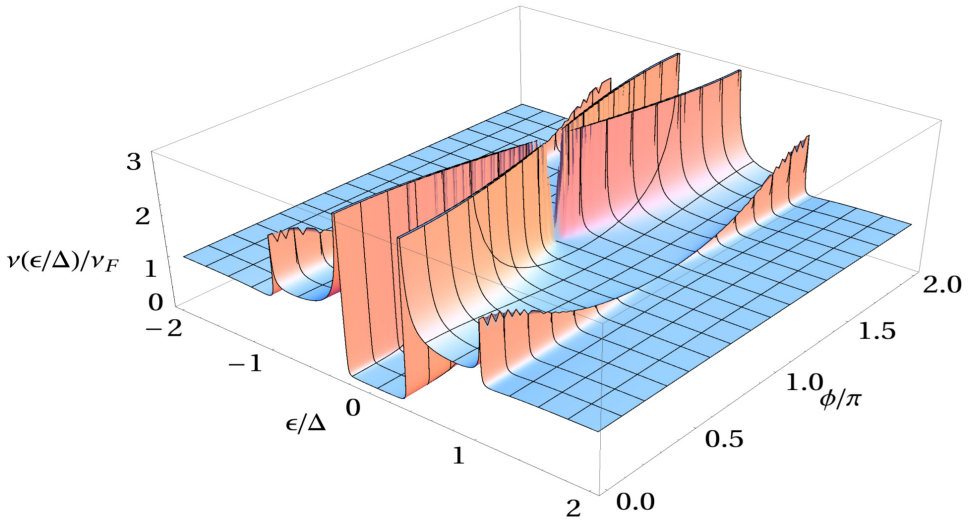

Figure 5.2: Density of states, $\nu(\epsilon)$, in the normal node for the STNTS case with $g = 0.2$, plotted against the phase difference between the superconducting reservoirs, ϕ. The proximity effect, in which a minigap in ν "leaks" into the normal metal from the superconductors, is clearly seen. The valleys above the minigap and below the gap in the superconductors, $|\Delta|$, result from scattering due to the impurities in the normal metal.

Using a single node has the advantage of not requiring iteration since the Green's functions of the reservoirs are known. After finding $\hat{R}_1$ in the node, the advanded Green's function is found from $\hat{A} = -\hat{\eta}_3 \hat{R}^\dagger \hat{\eta}_3$ and then the Keldysh component is found from eq. 3.34, $\hat{K} = (\hat{R} - \hat{A}) \tanh(\epsilon/2T)$. The density of states, $\nu(\epsilon)$, and the current can then be calculated using eqs. 4.12 and 4.13.

The density of states, $\nu(\epsilon)$, calculated from eq. 4.12 for parameter $g = 0.2$, is plotted in figure 5.2 against energy, ϵ, and against the phase difference, ϕ, across the junction. Of note is that the gap in ν disappears as the phase difference $\phi \to \pi/2$. Also of note is that there are no sharp Andreev peaks inside $-|\Delta| < \epsilon < |\Delta|$. They are instead spread out in the valleys shown. This spreading is due to the high concentration of impurities in the normal metal.

Figure 5.3 shows ν for $\phi = 0$ plotted against ϵ and g. For given σ_N, A, and ξ_N, decreasing g corresponds either to increasing R_T, i.e. making the tunnel resistances stronger, or to increasing the length of the junction, since the parameter $g \propto (R_T L)^{-1}$. Both cases may be seen as increasing an *effective* length of the junction because increasing R_T will cause particles

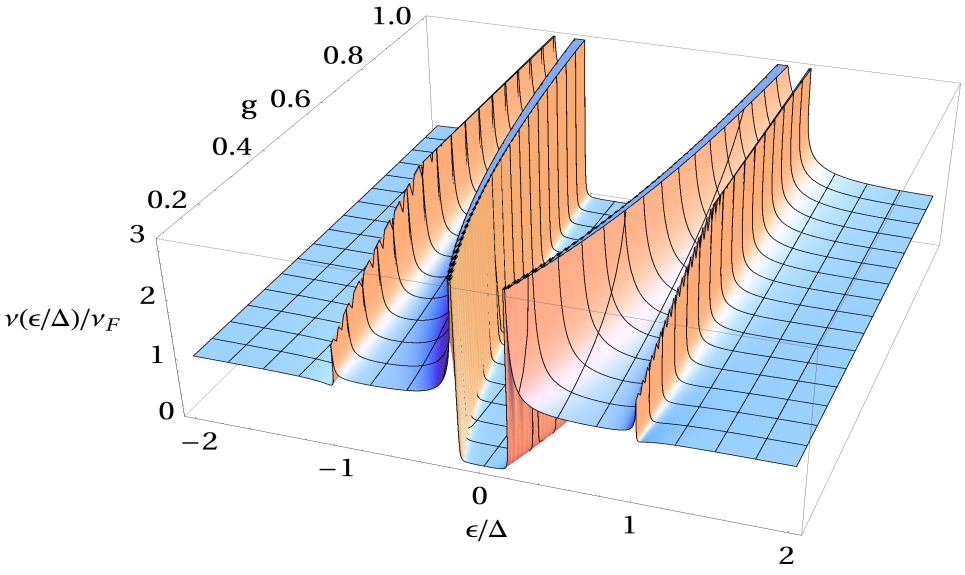

Figure 5.3: Density of states $\nu(\epsilon)$ in the normal node for the STNTS case with $\phi = 0$ plotted against the parameter g. The widening of the valleys for decreasing g results from the increased amount of scattering inherent in decreasing g.

to reflect more inside the junction thereby causing them to travel a greater distance in the wire before leaving. The parameter g is thus inversely related to this effective length. Figure 5.3 then shows that the gap is reduced as the effective length is increased.

5.2 Short SNS Junction

5.2.1 Tunnel junction model

Now let us turn to the other type of SNS setup studied here: a diffusive normal metal wire connecting two superconducting reservoirs. The code developed so far in this work, alas, is based entirely upon tunnel junctions. In the present system, however, there are no obvious tunnel junctions. How can one then model the diffusive wire using the code developed? This is in fact simply accomplished by modelling the diffusive wire as a series of tunnel junction connectors of equal conductances. The reason a tunnel junction may be imagined to be within the diffusive wire is that the diffusive wire itself may be considered as a series of many tunnel junctions of equal conductances [9]. This can be seen from the $\check{I} = i\mathcal{I}(\check{\phi})$ form of the matrix current from eq. 4.6. Using the simplest possible Green's function satisfying

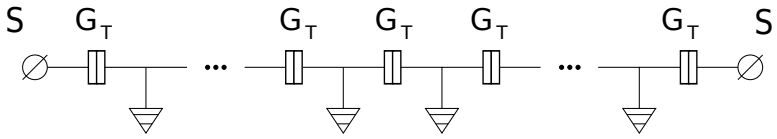

Figure 5.4: The quantum circuit theory model of a diffusive wire as many discrete nodes separated by tunnel junctions of equal conductance.

$\check{G}^2 = \check{1}$,

$$\check{G}_{1,2}(\phi_{1,2}) = \begin{pmatrix} 0 & \exp(i\phi_{1,2}) \\ \exp(-i\phi_{1,2}) & 0 \end{pmatrix}, \tag{5.1}$$

allows the transmission distribution function to be easily related to a matrix structure [9]. Such Green's functions are just a tool for getting some insight, and so the "*phases*", $\phi_{1,2}$, do not represent anything physical. Using eq. 5.1 to solve $\check{\phi} = -i\ln(\check{G}_1\check{G}_2)$ gives $\check{\phi} = i\check{\eta}_3(\phi_1 - \phi_2)$. The matrix current then takes the simple form $\check{I} = \check{\eta}_3\mathcal{I}(\phi)$ where now $\phi = \phi_1 - \phi_2$ is simply a scalar. The function $\mathcal{I}(\phi)$ from eq. 5.1, provided again here for reference is

$$\mathcal{I}(\phi) = G_Q \sum_p \frac{T_p \sin\phi}{1 - T_p \sin^2(\phi/2)}. \tag{5.2}$$

Writing this instead as an integral with a transmission distribution function, $\mathcal{I}(\phi)$ becomes

$$\mathcal{I}(\phi) = G_Q \int_0^1 \rho(T) \frac{T\sin(\phi)}{1 - T\sin^2(\phi/2)} dT. \tag{5.3}$$

Equation 5.3 indicates that if the transmission distribution of a connector is known then the phase dependence of the current, $\mathcal{I}(\phi)$, is also known. This equation can be inverted so that if the $\mathcal{I}(\phi)$ relation is instead known, then $\rho(T)$ can be found uniquely. The equation for this is

$$\rho(T) = \frac{\rho_D(T)}{\pi G} \operatorname{Re}\left(\mathcal{I}(\pi - 0 + 2i\cosh^{-1}(T^{-1/2}))\right);$$

$$\rho_D(T) = \frac{G_D}{2G_Q T\sqrt{1-T}},$$

where $\rho_D(T)$ is known to be the transmission distribution for a diffusive connector of conductance G_D.

Since the focus of this section is to model a diffusive conductor, note that using $\rho_D(T)$ in eq. 5.3 gives a linear $\mathcal{I}$-ϕ relation for a diffusive connector:

$$\mathcal{I}(\phi) = G_D\phi. \tag{5.4}$$

As mentioned, a method of modelling the diffusive connector is to have a large number, N, of identical tunnel junctions in series. In such a case,

each tunnel junction has the same $\mathcal{I}$-ϕ relation, labelled $\mathcal{I}_0(\phi)$ for clarity. Assigning to each of the $N-1$ nodes a phase θ_i, $i = 1, 2, ..., N-1$, current conservation then implies that $\mathcal{I}_0(\theta_i - \theta_{i-1})$ across each connector is the same, i.e.

$$\mathcal{I}_0(\phi - \theta_1) = \mathcal{I}_0(\theta_1 - \theta_2) = ... = \mathcal{I}_0(\theta_{N-2} - \theta_{N-1}) = \mathcal{I}_0(\theta_{N-1}).$$

Since all connectors are equivalent, the difference $\theta_i - \theta_{i-1}$ across each connector is then $\theta_i - \theta_{i-1} = \phi/N$ and the overall $\mathcal{I}$-ϕ characteristic for the structure is given by $\mathcal{I}(\phi) = \mathcal{I}_0(\phi/N)$. From the form of eq. 5.2, $\mathcal{I}_0(\phi/N)$ is linear in ϕ for large N according to

$$\mathcal{I}(\phi) = \mathcal{I}_0(\phi/N) \approx G_D\phi; \quad G_D = N^{-1}G_Q \sum_p T_p.$$

The $G_Q \sum_p T_p$ part of the conductance G_D is recognised as the tunnel conductance, G_T, from eq. 4.5. The point here is that the long series of connectors provides, for large N, the same linear $\mathcal{I}(\phi)$ relation as a diffusive connector. Since the $\mathcal{I}$-ϕ relation unambiguously gives $\rho(T)$, the chain of many connectors thus approximates the diffusive transmission distribution, $\rho_D(T)$. The diffusive connector can thus be regarded as simply a series of many (large N) identical tunnel junctions of tunnel conductance $G_T = NG_D$. This is why the tunnel junction "nodecode" can be used to model the diffusive wire.

5.2.2 Derivation of KO1 equation

The starting point in deriving the KO1 current expression is to neglect the non-gradient terms in the Usadel equation [20]. This corresponds to neglecting the leakage current in eq. 3.39. The Usadel equation becomes

$$\nabla_{\boldsymbol{R}} \cdot \check{\boldsymbol{j}} = 0; \; \check{\boldsymbol{j}} = -\sigma \; \check{G}\nabla_{\boldsymbol{R}}\check{G},$$

exactly conserving matrix current. Since the leakage current accounts for decoherence of particles and holes and the conversion of cooper pairs to quasiparticles, the no leakage assumption is that the junction is so much shorter than the coherence length, ξ_N, that the particles do not have enough time in the normal region to lose coherence or be converted to quasiparticles. In appendix B, a general expression for the matrix current, $\check{I}$, in the absence of leakage current is derived and given as eq. B.7. The result is

$$\hat{I} = G_D \ln(\hat{G}_1\hat{G}_2),$$

where the hats are used since the Matsubara technique with 2x2 matrices is used in the following derivation. The quantity $\ln(\hat{G}_1\hat{G}_2)$ is recognised as the

matrix phase from eq. D.1, $\hat{\phi} = -i \ln(\hat{G}_1 \hat{G}_2)$. The current may therefore be written as

$$\hat{I} = i G_D \hat{\phi},$$

in agreement with eq. 5.4 for a diffusive conductor. The KO1 current equation can be simply derived using the expression for $\hat{\phi}$ in eq. E.2, as well as other results given in appendix E. The expression for $\hat{\phi}$ is, for reference,

$$\hat{\phi} = -2 \tan^{-1} \left(\sqrt{\frac{1-\Theta}{1+\Theta}} \right) \hat{P} \hat{\eta}_3 \hat{P}^{-1},$$

where

$$\Theta(\zeta_n) \equiv \mathrm{Tr}(\hat{G}_1 \hat{G}_2)/2,$$

and $\hat{P} \hat{G}_1 \hat{G}_2 \hat{P}^{-1}$ is diagonal. The expression for the current is

$$I_M = \mathrm{Im} \left[\frac{i\pi}{e} G_D T \sum_{\zeta} \tan^{-1} \left(\sqrt{\frac{1-\Theta}{1+\Theta}} \right) \mathrm{Tr}(\hat{\eta}_3 \hat{P} \hat{\eta}_3 \hat{P}^{-1}) \right]. \tag{5.5}$$

The KO1 result is for two equal superconducting reservoirs at equilibrium, so the usual reservoir Green's functions are used in the following. Using the results of appendix E, the trace evaluates to

$$\mathrm{Tr}(\hat{\eta}_3 \hat{P} \hat{\eta}_3 \hat{P}^{-1}) = \frac{2 \cos(\phi/2)}{\delta}$$

while

$$\sqrt{\frac{1-\Theta}{1+\Theta}} = \frac{|\Delta| \sin(\phi/2)}{\delta},$$

where $\delta \equiv \sqrt{\zeta_n + |\Delta|^2 \cos^2(\phi/2)}$. Inserting these into the current expression eq. 5.5 gives the KO1 current relation [20]:

$$I_M(\phi, T) = \frac{4\pi T}{e R_D} \sum_{\zeta_n > 0} \frac{|\Delta| \cos(\phi/2)}{\delta} \arctan \frac{|\Delta| \sin(\phi/2)}{\delta}, \tag{5.6}$$

where a factor 2 was extracted by using the symmetry of the sum over Matsubara frequencies.

5.2.3 Results of the TJ model

Having the KO1 equation now at hand, the tunnel junction model may be applied to the short diffusive junction and compared with theory. The KO1 theory uses the approximation of no leakage current. To match the results of the theory while keeping the same code including leakage current, a very large value for g should be used to make the leakage current negligible. This corresponds also to the notion that $L \ll \xi_N$. Accordingly, g was set to

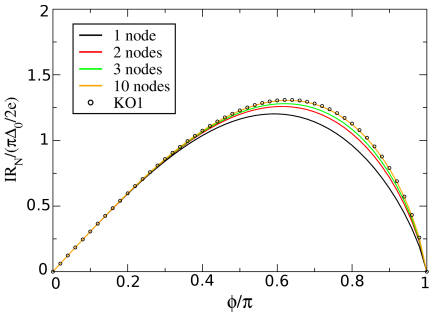

Figure 5.5: Current-phase relation for multinode chains at $T/T_c = 1/100$ compared to KO1 result.

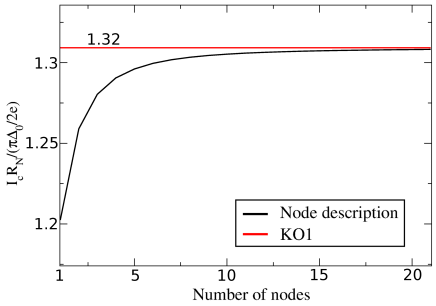

Figure 5.6: Convergence of the "nodecode" towards the KO1 result as the number of nodes (the fineness of the discretisation) is increased.

$g = 10^6$ for the following calculations. Since no true junction has zero length, the nodecode with a fine enough discretisation may provide more accurate results than the KO1 theory. Figure 5.5 shows the CPR for $T/T_c = 1/100$, calculated using the tunnel junction model, compared with the corresponding KO1 result. Using a single node, the tunnel junction model provides roughly the same features as theory. Increasing the number of nodes brings the result closer and closer to the theoretical result, exhibiting agreement within 1% for 10 nodes. Figure 5.6 shows how the tunnel model result converges to the KO1 result as the number of nodes is increased.

The tunnel junction model succeeds also in reproducing the correct I_c-T relations. This is shown in figure 5.7. Once again the results are better for greater numbers of nodes. In this case, one sees that fewer nodes are required to achieve good results for higher temperatures than for lower temperatures.

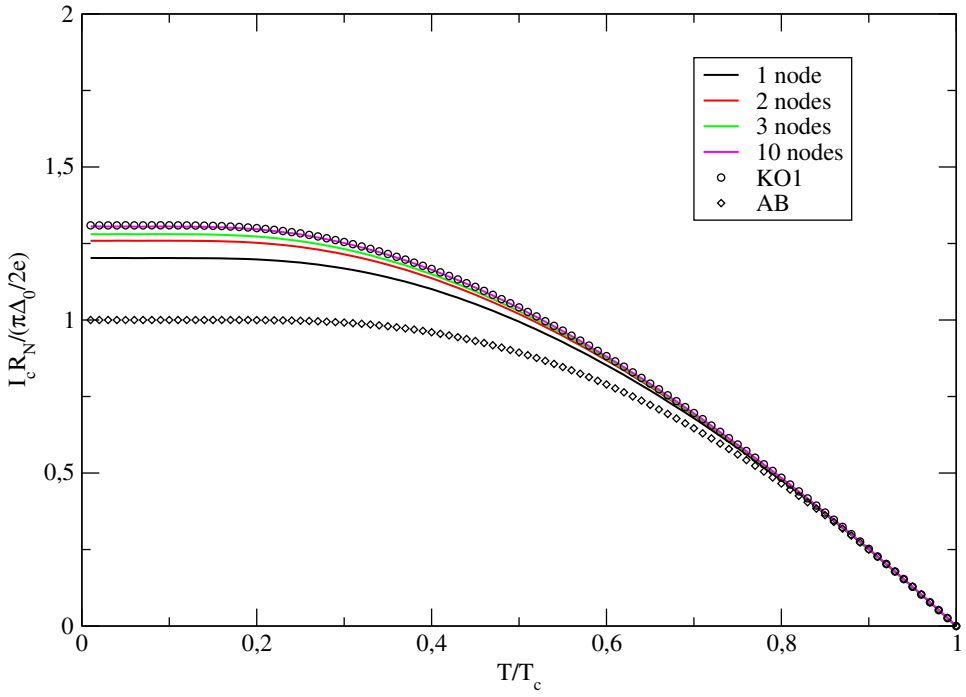

Figure 5.7: Critical current vs. temperature for the many-node model of the short diffusive wire compared to the KO1 result as well as the Ambegaokar-Baratoff (AB) result for a single tunnel junction.

5.3 SS'S

With the code working for the SNS case, a natural extension is for cases where the intermediate metal has an attractive coupling. Two cases arise where the temperature, T, is either below or above the superconducting critical temperature $T_{c'}$ of the intermediate metal so that it may be either superconducting or not. In this work, only the case where the intermediate metal is of the same type as the reservoirs is considered so that $T_c = T_{c'}$. Compared to the SNS case, the superconductivity in the intermediate metal poses an additional challenge; the Hamiltonian term, $\check{E}$, in the leakage current now contains a non-zero energy gap $|\Delta| \neq 0$. Care must be taken in dealing with the order parameter Δ, because simple intuition will likely produce incorrect results. The problems with intuitive assumptions about the size and phase of the order parameter are illustrated in sections 5.3.1 and 5.3.2. In section 5.3.3, a procedure to obtain correct results is described and applied.

5.3.1 Problem 1: periodicity

Consider the STNTS case as in section 5.1 but now with a superconducting metal in the junction (STSTS). Given that the intermediate material is the same as the reservoirs, an intuitive guess for the order parameter on the node would be that it have the same magnitude as the reservoirs and that the total change in the phase is distributed equally between the two connectors. Figure 5.8 shows the I-ϕ relation (or CPR for Current-Phase Relation) of this single node circuit under the above assumptions for different values g of the intermediate metal.

Josephson junctions have 2π-periodicity in the CPR. The present assumptions shown in fig. 5.8 clearly deviate from this. The CPR proved instead to be 4π-periodic. This is not correct. One may consider that the error is due to the relatively long effective lengths plotted. The approach of circuit theory is then to discretise the intermediate metal further to account for the rapid changes in the $\check{G}$'s on the scale of ξ_N. This possible resolution is examined in the following section.

5.3.2 Problem 2: current conservation

To remedy the non-2π periodicity of the SSS junction examined above, one can try discretising the system further using the same approach as in section 5.2. This should better account for the rapid changes in the Green's functions on the scale of ξ_N. Keeping the same intuitive assumptions as above the phase is assumed to drop an equal amount across each connector. The size of the energy gap is again assumed to be the same everywhere. Results from this approach using five nodes are shown in figure 5.9. As

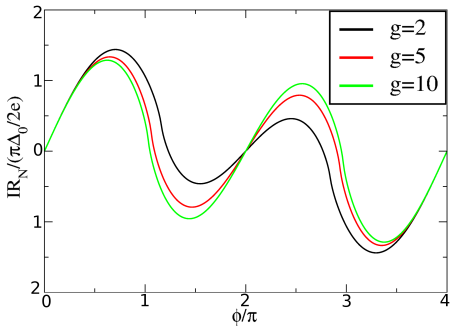

Figure 5.8: $I-\phi$ for STSTS for g =2,5, and 10. Junctions of this type are known to have 2π periodic $I-\phi$ relations. This is clearly not the case here under the present assumptions.

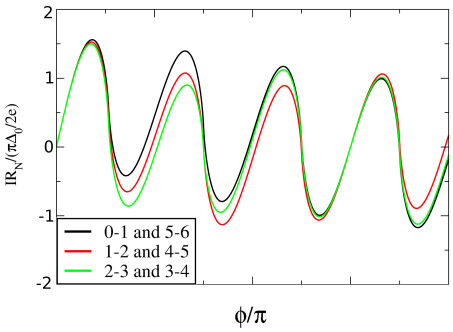

Figure 5.9: CPR for SSS discretised into 5 nodes using intuitive assumptions for Δ. The plot shown is for $g = 2$. Not only is the 2π-periodicity not recovered but also the multi-node approach exhibits non-conservation of current.

can be seen, discretising the system more thoroughly does not restore the required 2π-periodicity to the CPR. Not only that but by having multiple nodes also shows that the assumptions have led to non-conservation of current. As there is no actual leakage of current anywhere in the system, better discretisation is not the solution to the errors in the CPR. Self-consistency of the order-parameter has not been accounted for under the present assumptions. Current conservation in superconductors requires self-consistency so it might be expected to solve at least the non-conservation of current problem. Incorporating self-consistency into the circuit theory is the topic of the next section.

5.3.3 Solution: self-consistency

Self-consistency is generally required for current-conservation in superconductors. It is clearly a potential solution, at least to the current-conservation problem of section 5.3.2. A self-consistent order-parameter can be added straightforwardly to the circuit theory algorithm. First, Green's functions are calculated as usual according to the circuit theory algorithm. Once the Green's functions have relaxed to the desired accuracy, the order parameter in each node is calculated from the anomalous component of the Green's function of each node according to eq. 3.28,

$$\Delta = \frac{i\pi T \sum_{n=-n_c}^{n_c} \langle [\hat{\mathcal{G}}^M]_{12}(\boldsymbol{R}, \hat{\boldsymbol{p}}, \zeta_n) \rangle}{\ln\left(\frac{T}{T_c}\right) + \sum_{n=0}^{n_c} \frac{1}{|\zeta_n|}}.$$

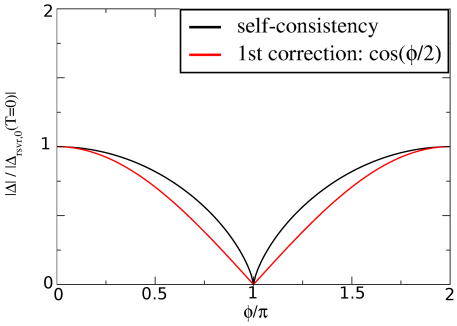

Figure 5.10: Magnitude of the gap, $|\Delta|$, for a single node, vs. phase difference ϕ for the STSTS circuit.

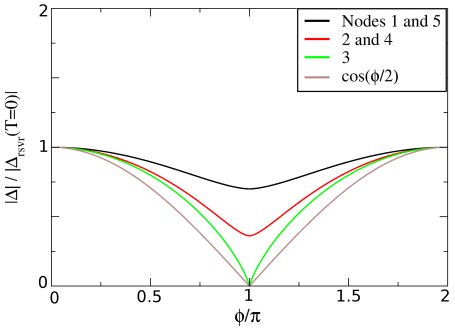

Figure 5.11: The gap sizes in the 5 nodes when discretising the intermediate metal in the STSTS circuit into 5 nodes.

The node-code is then run again but this time using the updated order-parameter. This procedure is repeated until the order parameter has relaxed to the desired accuracy. At this point, observables from the resulting Green's functions can be calculated as usual. An initial guess for the order-parameter is required. In this work $\Delta = 0$ was used as the guess.

Figure 5.10 shows the magnitude of the order-parameter for a single node circuit, $|\Delta|$, when calculated self-consistently. That $|\Delta|$ varies with respect to ϕ is seen immediately, a feature not incorporated in the intuitive assumption which assumed $|\Delta| = |\Delta_{res}| \not\propto \phi$. The first iteration result of the self-consistency calculation with the guess $|\Delta| = 0$ is also shown for comparison. This first iteration corresponds to $\Delta = (\Delta_L + \Delta_R)/2$, the average of the order-parameters of the left and right reservoirs. Taking such an average is clearly a better approximation for this single-node case to the full self-consistent calculation than the initial intuitive guess.

The result for the five node case is shown in figure 5.11. The size of the gap again changes with ϕ but the effect is more pronounced as the center node is approached. The behaviour of the center node is the same as for the node in the single-node case above.

Finally, the CPR for the five node case is shown in figure 5.12. The figure shows clearly that both the problems of sections 5.3.1 and 5.3.2 have been solved by the implentation of the self-consistent order parameter algorithm; both the 2π-periodicity and current conservation have been restored.

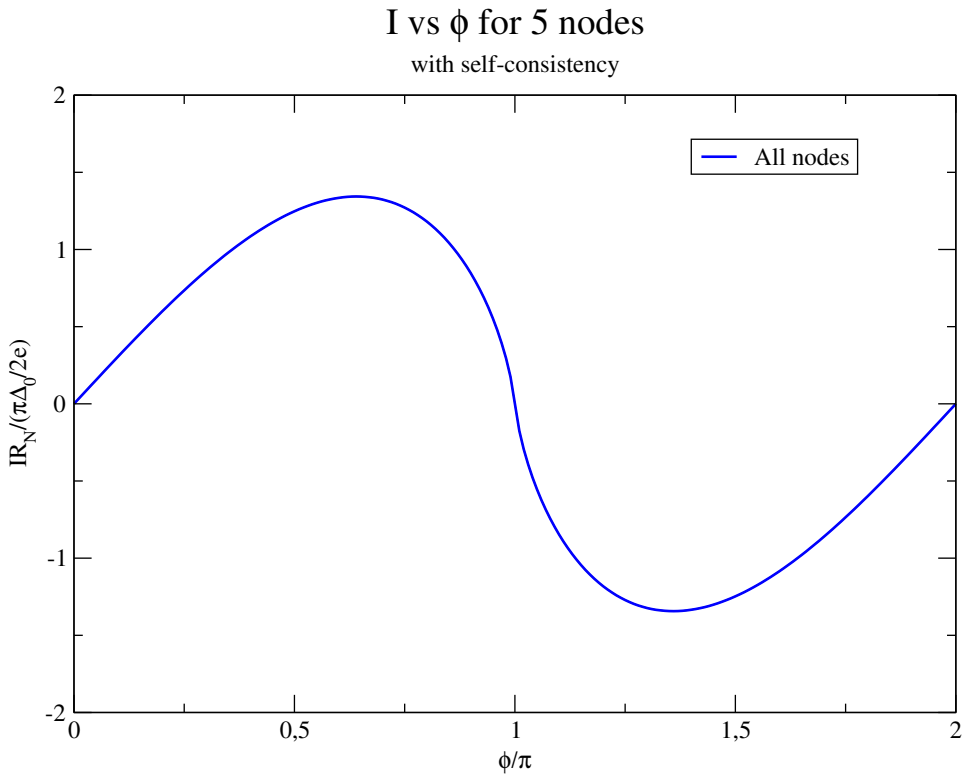

Figure 5.12: CPR for the 5 node model of an STSTS junction. Both 2π-periodicity and current conservation are restored by adding self-consistency to the algorithm.

Chapter 6

Conclusions and Outlook

Much of the thesis work was literature review of quasiclassical methods in superconductivity and Nazarov's circuit theory. The most relevant parts of this review were presented in chapters 2 to 4. The quantum circuit theory was derived from the Usadel equation, eq. 4.1, in a manner analogous to how classical circuit theory is derived from Laplace's equation, eq. 2.7. Quantum circuit theory is important as an alternative to the Usadel equation which is known to be difficult to solve analytically and numerically. It offers instead a discrete element method of solution that is relatively easy to solve numerically and occasionally analytically.

The aim of this thesis project was originally to model the Andreev interferometer shown in figure 1.1 using quantum circuit theory. This remains to be done but the most fundamental of the building blocks which arise from discretising the interferometer were modelled. The STNTS case showed that stronger tunnel barriers destroy the superconducting proximity effect in the normal metal. It also exhibited the correct behaviour for density of states with phase, ϕ, the gap closing at $\phi = \pi$. The short diffusive wire case studied by Kulik and Omelyanchuk was also modelled using QCT. Using only tunnel junctions as connectors, the circuit theory converged to the KO1 result as the number of nodes is increased, reaching accuracy of within %1 with as few as 10 nodes. The model exhibited the correct I-ϕ and I_c-T relations and showed that fewer nodes are required for accuracy at temperatures close to T_c than at lower temperatures. The SSS junction case added complications to the circuit theory in that, without a self-consistently determined order parameter $\Delta(\boldsymbol{R})$, incorrect results were obtained for I-ϕ: 2π-periodicity and current conservation were lost. Applying the self-consistency algorithm described in section 5.3.3 resolved both problems without adding much complexity to the program code.

Outlook

The first steps towards modelling the complete Andreev interferometer using quantum circuit theory were laid out in this work. In studies of Andreev interferometers to date, the superconducting parts of the ring are usually regarded as bulk (as in [13]), ignoring changes in the order parameter within these regions. For the Andreev interferometer depicted in Fig. 1.1, these regions are too small to be considered as bulk. To describe them accurately one may be able to model them as SSS junctions using quantum circuit theory. The self-consistency algorithm developed in this work for the SSS type junction should work nicely for this purpose. The current that is pushed through the interferometer needs also to be incorporated into the theory. This will require the inclusion of the magnetic vector potential, $\boldsymbol{A}(\boldsymbol{R})$. In any case, quantum circuit theory offers an interesting and powerful means of considering such complex structures as the Andreev interferometer.

Appendix A

Useful implications of $\check{G}^2 = \check{1}$

In this section some simple but useful relations for quasiclassical Green's functions are derived for reference from the normalisation condition, $\check{G}^2 = \check{1}$.

Given the Green's functions at two different points, $\check{G}_1$ and $\check{G}_2$ we have clearly then that

$$\check{G}_1^2 = \check{G}_2^2 = \check{1}.$$

This allows the following:

$$\check{G}_1^2 = \check{G}_1(\check{G}_2\check{G}_2)\check{G}_1 = \check{1}.$$

Clearly then,

$$\check{G}_1\check{G}_2 = (\check{G}_2\check{G}_1)^{-1}. \tag{A.1}$$

It is also clear that

$$[\check{G}_1\check{G}_2, \check{G}_2\check{G}_1] = \check{1} - \check{1} = 0, \tag{A.2}$$

so that $\check{G}_1\check{G}_2$ and $\check{G}_2\check{G}_1$ commute. Two matrices that commute are simultaneously diagonalisable.

Further useful relations come from considering the anticommutator of the sum and difference of $\check{G}_1$ and $\check{G}_2$:

$$\{(\check{G}_1 + \check{G}_2), (\check{G}_1 - \check{G}_2)\} = 0. \tag{A.3}$$

Now consider that $\{\check{G}_1, (\check{G}_2 - \check{G}_1)\} \to 0$ in the limit $\check{G}_2 \to \check{G}_1$. Since any derivative of $\check{G}$ is based on this type of limit we have that differential variations of $\check{G}$ anticommute with $\check{G}$, i.e. that

$$\{\check{G}, \nabla\check{G}\} = 0. \tag{A.4}$$

Appendix B

No leakage current

In cases where $[\check{E}, \check{G}] = 0$, there is no leakage current. No leakage current implies consequently that the Green's function may be rewritten everywhere as $\check{G}(\boldsymbol{r}) = a(\boldsymbol{r})\check{E}(\boldsymbol{r})$ where a is a scalar function of $\boldsymbol{r}$. Taking the gradient in $\boldsymbol{r}$-space of $\check{G}$ gives

$$\nabla\check{G} = \frac{(\nabla a)}{a}\check{G} + a\nabla\check{E}. \tag{B.1}$$

Left and right multiplying eq. B.1 by $\check{G}$ and taking the difference gives:

$$-2(\nabla\check{G})\check{G} = \check{G}\nabla\check{G} - (\nabla\check{G})\check{G} = a[\check{G}, \nabla\check{E}].$$

As a result

$$\nabla\check{G} = -\check{\boldsymbol{U}}\check{G}, \tag{B.2}$$

where $\check{\boldsymbol{U}}$ is a matrix of vectors defined as

$$\check{\boldsymbol{U}} = \frac{a}{2}[\check{G}, \nabla\check{E}]\check{G} = -\check{G}\nabla\check{G} = \check{\boldsymbol{j}}/\sigma(\boldsymbol{r}). \tag{B.3}$$

Consider a terminal connected at $\boldsymbol{r}_1$ where $\check{G}(\boldsymbol{r}_1) = \check{G}_1$. Since $\nabla G_1 = 0$, eq. B.2 has a solution of the form

$$\check{G}(\boldsymbol{r}) = \exp(\check{L})\ \check{G}_1,$$

where $\check{\boldsymbol{U}} = -\nabla\check{L}$. The normalisation condition requires then that $\{\check{L}, \check{G}_1\} = 0$ and subsequently $\check{L} = u(\boldsymbol{r})\check{M}$ where u is a scalar function and $\check{M}$ is a constant matrix that anticommutes with $\check{G}_1$. We now have that $\check{\boldsymbol{U}} = -\nabla u(\boldsymbol{r})\check{M}$ and further that

$$\check{\boldsymbol{j}} = -\sigma(\boldsymbol{r})\nabla u(\boldsymbol{r})\check{M}. \tag{B.4}$$

Given the form of the matrix current density $\check{\boldsymbol{j}} = \sigma(\boldsymbol{r})\check{\boldsymbol{U}}$, which is recognised as analogous to Ohm's law, the scalar function $u(\boldsymbol{r})$ must be related to the electric potential per unit energy. Suppose the values of u at the terminal

at $\boldsymbol{r}_1$ and at another point, $\boldsymbol{r}_2$, in the nanostructure are known: $u(\boldsymbol{r}_1) = 0$ and $u(\boldsymbol{r}_2) = 1$. The matrix $\check{M}$ may then be found from $\check{G}_2 = \exp((u(\boldsymbol{r}) = 1)\check{M})\check{G}_1$, giving

$$\check{M} = \ln(\check{G}_2\check{G}_1) = -\ln(\check{G}_1\check{G}_2). \tag{B.5}$$

The Usadel equation now takes the form

$$\nabla \cdot (\sigma \nabla u \check{M}) = 0. \tag{B.6}$$

Integrating the matrix current density in eq. B.4 over a cross-section gives the matrix current through that cross-section as

$$\check{I} = G_D \ln(\check{G}_1\check{G}_2), \tag{B.7}$$

where G_D is the proportionality factor of the current through the chosen cross-section to the total current, i.e. the conductance of the material.

Appendix C

Usadel equation analysis of 1D normal metal wire

In this section, charge and heat transport in a normal 1D wire are examined using the Usadel equation. As there are no superconductors present, only 2×2 matrices are required. For a normal metal then $\check{E} = \epsilon\check{1}$ so that $[\check{E}, \check{G}] = 0$ allowing use of the results of section B.

C.1 Distribution function and electric current

Assuming the metal to have homogeneous conductivity $\sigma(\boldsymbol{r}) = \sigma$, the Usadel equation (eq. B.6) becomes simply $\nabla^2 u = 0$. The function u takes the general form $u = Ax + C$ where A and C are constants. Boundary conditions may be set as normal terminals at $x = 0, L$, at the ends of the wire, so that $u(0) = 0$ and $u(L) = 1$. This gives $A = 1/L$ and $C = 0$, i.e.

$$u(x) = x/L.$$

Using the form of the Green's function from appendix B,

$$\check{G}(x) = \exp(u(x)\check{M})\check{G}_0.$$

An expression for the matrix $\check{M}$ is needed. The Keldysh Green's functions in the terminals are known to be

$$\check{G}_{0,L} = \begin{pmatrix} 1 & 2(1 - 2f_{0,L}) \\ 0 & -1 \end{pmatrix},$$

where $f_{0,L} = f_F(\epsilon + \mu_{0,L})$ and f_F is the usual Fermi distribution.

The equation for the matrix $\check{M}$ is $\check{M} = -\ln(\check{G}_0\check{G}_L)$. After Jordan decomposition, rewrite $\check{G}_0\check{G}_1 = \check{S}\check{J}\check{S}^{-1}$, where

$$\check{S} = \begin{pmatrix} 1 & 0 \\ 0 & (f_0 - f_L)/4 \end{pmatrix}$$

and the Jordan block, $\check{J}$, is

$$\check{J} = \begin{pmatrix} 1 & 1 \\ 0 & 1 \end{pmatrix}.$$

Using the identity for an invertible matrix Y, $\ln(YXY^{-1}) = Y\ln(X)Y^{-1}$ gives

$$\check{M} = \begin{pmatrix} 0 & -4(f_0 - f_L) \\ 0 & 0 \end{pmatrix}.$$

Since $\check{M}^2 = 0$, the matrix Green's function in the wire is simply

$$\check{G}(x) = (\check{1} + u(x)\check{M})\check{G}_1.$$

To find the distribution function in the wire as a function of position, only the Keldysh component of the Green's function is needed, since its form is known for a normal metal (when using only 2×2 matrices) to be

$$K = Rh - hA = (R - A)h;\ h = 1 - 2f.$$

Solving for f gives

$$f(x) = \frac{1}{2}\left(1 - \frac{K}{R - A}\right).$$

From above, the Keldysh component is $K = 1 - 4(f_0 - f_L)u(x)$ so, since $R - A = 2$ and $u(x) = x/L$, the distribution function in the wire is

$$f(x) = \left(\frac{L - x}{L}\right) f_L + \left(\frac{x}{L}\right) f_R.$$

The electric current density is

$$\boldsymbol{j} = \frac{\sigma}{L}(f_0 - f_L),$$

since $\boldsymbol{j} = \frac{\mathrm{Tr}(\check{\boldsymbol{j}}^K}{4})$. Assuming a potential difference, V, between $x = 0$ and $x = L$ and then integrating over energy gives the total current as

$$I = gV,$$

where $g = \sigma/L$ is the linear conductance of the nanowire.

C.2 Wiedemann-Franz law

The current density $\boldsymbol{j}$ found in the previous section can be used further to investigate heat transport in the wire. The heat current density is given by

$$\boldsymbol{Q} = \frac{1}{e^2}\int_{-\infty}^{\infty} E\boldsymbol{j}dE.$$

Using the previous result $\boldsymbol{j} = \sigma/L(f_0 - f_L)$ and switching back $E \to E - E_F$ produces

$$\boldsymbol{Q} = \frac{\sigma \hat{\boldsymbol{x}}}{e^2 L} \int_0^\infty (E - E_F)(f_0 - f_L) dE.$$

Assuming no applied potential difference, but a small temperature gradient, $\Delta T = T_1 - T_2$, $f_0 - f_L$ can be expanded in powers of ΔT about T_1:

$$(f_0 - f_L) \approx -\frac{(E - E_F) \exp\left(\frac{E-E_F}{kT}\right) \Delta T}{\left(1 + \exp\left(\frac{E-E_F}{kT}\right)\right)^2 kT^2}.$$

A factor 2 is required to account for the spins of the particles. Using the trigonometric identity

$$\mathrm{e}^{\mathrm{x}} + \mathrm{e}^{-\mathrm{x}} + 2 = 2(\cosh \mathrm{x} + 1) = 4 \cosh \frac{\mathrm{x}}{2},$$

and that

$$\int_0^\infty \frac{x^2 dx}{\cosh^2 x} = \frac{\pi^2}{12},$$

gives

$$Q = -\kappa \Delta T; \quad \kappa \equiv \frac{\pi^2}{3} \frac{\sigma}{e^2} k_B^2 T,$$

where κ is the thermal conductivity. This exhibits the Wiedemann-Franz law for the ratio of the thermal and electric conductivities:

$$\frac{\kappa}{\sigma T} = \frac{\pi^2 k_B^2}{3e^2}.$$

Appendix D

Rewriting $\check{I}$ as function of $\check{\phi}$

This appendix shows how to transform the boundary condition for connectors,

$$\check{I} = G_Q \sum_p \frac{T_p[\check{G}_1, \check{G}_2]}{2 + \frac{T_p}{2}(\{\check{G}_1, \check{G}_2\} - 2)},$$

to being written in terms of the "matrix phase" $\check{\phi} = -i \ln(\check{G}_1 \check{G}_2)$.

Since $(\check{G}_1 \check{G}_2)^{-1} = \check{G}_2 \check{G}_1$, the commutator $[\check{G}_1, \check{G}_2]$ may be rewritten in the form $[\check{G}_1, \check{G}_2] = \exp(i\check{\phi}) - \exp(-i\check{\phi})$, where the matrix phase, $\check{\phi}$, is defined

$$\check{\phi} \equiv -i \ln(\check{G}_1 \check{G}_2). \tag{D.1}$$

Using $2i \sin \check{\phi} = \exp(i\check{\phi}) - \exp(-i\check{\phi})$ gives $[\check{G}_1, \check{G}_2] = 2i \sin \check{\phi}$. Similarly, $2 \cos \check{\phi} = \{\check{G}_1, \check{G}_2\}$. The matrix current now takes the form

$$\check{I} = iG_Q \sum_p \frac{T_p \sin \phi}{1 - \frac{T_p}{2}(1 - \cos \check{\phi})}.$$

The denominator may be rewritten using the half-angle formula, $\sin^2(\check{\phi}/2) = (1 - \cos \check{\phi})/2$, leading to the final result:

$$\check{I} = i\mathcal{I}(\check{\phi}); \quad \mathcal{I}(\phi) = G_Q \sum_p \frac{T_p \sin \phi}{1 - T_p \sin^2(\phi/2)}.$$

Appendix E

Diagonalising $\check{G}_1\check{G}_2$

The form of the matrix current $\check{I} = i\mathcal{I}(\check{\phi})$ containing the matrix phase, $\check{\phi} = -i\ln(\check{G}_1\check{G}_2)$, is tricky to use for practical calculations containing real Green's functions. By diagonalising the matrix $\check{G}_1\check{G}_2$, however, $\check{\phi}$ may be cast into another form that may be useful. This relies on the identity for the matrix logarithm $\ln(YXY^{-1}) = Y\ln(X)Y^{-1}$, given matrix Y is invertible. The matrix $\check{G}_1\check{G}_2$ is known to be diagonalisable due to equation A.2. The derivation follows the usual method of diagonalising a matrix, by finding the matrices $\check{P}$ and $\check{D}$ such that $\check{P}^{-1}\check{G}_1\check{G}_2\check{P} = \check{D}$ where $\check{D}$ is a diagonal matrix composed of the eigenvalues of $\check{G}_1\check{G}_2$ and $\check{P}$ is composed of the respective eigenvectors. The starting point is thus to find the eigenvalues, λ, from the equation

$$\det\begin{pmatrix}\hat{R}_1\hat{R}_2 - \hat{\lambda} & \hat{R}_1\hat{K}_2 + \hat{K}_1\hat{A}_2 \\ \hat{0} & \hat{A}_1\hat{A}_2 - \hat{\lambda}\end{pmatrix} = 0,$$

which reduces to $\det(\hat{R}_1\hat{R}_2 - \hat{\lambda})\det(\hat{A}_1\hat{A}_2 - \hat{\lambda}) = 0$. Solving gives the following set of 4 eigenvalues:

$$\lambda_{G,\pm} = \frac{\mathrm{Tr}(\hat{G}_1\hat{G}_2)}{2} \pm \frac{1}{2}\sqrt{2\,\mathrm{Tr}^2(\hat{G}_1\hat{G}_2) - 4},$$

where G is used as an index for either $\hat{R}$ or $\hat{A}$. The diagonal matrix $\check{D}$ may therefore be written

$$\check{D} = \begin{pmatrix}\hat{\lambda}_R & \hat{0} \\ \hat{0} & \hat{\lambda}_A\end{pmatrix}; \quad \hat{\lambda}_G = \begin{pmatrix}\lambda_{G+} & 0 \\ 0 & \lambda_{G-}\end{pmatrix}.$$

Using the eigenvalues to find the eigenvectors gives the diagonalising matrix $\check{P}$ as

$$\check{P} = \begin{pmatrix}\hat{P}_R & \hat{P}_K \\ \hat{0} & \hat{P}_A\end{pmatrix},$$

wherein

$$\hat{P}_G = \begin{pmatrix}[\hat{G}_1\hat{G}_2]_{12} & [\hat{G}_1\hat{G}_2]_{12} \\ \lambda_{G+} - [\hat{G}_1\hat{G}_2]_{11} & \lambda_{G-} - [\hat{G}_1\hat{G}_2]_{11}\end{pmatrix},$$

and

$$\hat{P}_K = \begin{pmatrix} [\hat{R}_1\hat{R}_2]_{12} & [\hat{R}_1\hat{R}_2]_{12} \\ [P_K]_{2+} & [P_K]_{2-} \end{pmatrix},$$

where

$$[P_K]_{2\pm} = -\frac{(\hat{\Phi}_{11}[\hat{P}_A]_{11} + \hat{\Phi}_{12}[\hat{P}_A]_{2(1,2)})}{[\hat{R}_1\hat{R}_2]_{12}} - ([\hat{R}_1\hat{R}_2]_{11} - \lambda_{A\pm}).$$

Finally, the matrix $\hat{\Phi}$ is defined

$$\hat{\Phi} = \hat{R}_1\hat{K}_2 + \hat{K}_1\hat{A}_2.$$

It is useful to note the form of $\hat{P}^{-1}$:

$$\hat{P}^{-1} = \begin{pmatrix} \hat{P}_R^{-1} & -\hat{P}_R^{-1}\hat{P}_K\hat{P}_A^{-1} \\ \hat{0} & \hat{P}_A^{-1} \end{pmatrix}.$$

Now the matrix phase can be written $\check{\phi} = -i\check{P}\ln(\check{D})\check{P}^{-1}$. The matrix logarithm of a diagonal matrix is just the same matrix but with each diagonal entry replaced by its natural logarithm. To compute the logarithm, any of the complex sinusoidal identities $\cos^{-1} z = -i\ln[z + (z^2-1)^{1/2}]$, $\sin^{-1} z = -i\ln[iz + (1-z^2)^{1/2}]$, and $2i\tan^{-1} z = \ln[(i-z)/(i+z)]$ may be used, depending on convenience. Using the $\sin^{-1} z$ and the $\tan^{-1} z$ identities puts $\check{\phi}$ respectively in the following forms:

$$\check{\phi} = -\check{P}\sin^{-1}(\sqrt{1-\Theta^2})\check{\eta}_3\check{P}^{-1} \tag{E.1}$$

$$\check{\phi} = -2\check{P}\tan^{-1}(\sqrt{(1-\Theta)/(1+\Theta)})\check{\eta}_3\check{P}^{-1}. \tag{E.2}$$

The function Θ is defined, following Nazarov,

$$\Theta(\epsilon) \equiv \mathrm{Tr}(\hat{R}_1\hat{R}_2)/2.$$

Although the form of $\check{I}$ given in eq. 4.4 is more useful for most applications, its form is given here in terms of $\check{P}$ and $\check{D}$ in accordance with the present context. Using eq. E.1 for $\check{\phi}$ in $\check{I} = i\mathcal{I}(\check{\phi})$ gives the matrix current as

$$\check{I} = \mathcal{Z}(\Theta)\sqrt{\Theta^2-1}\ \check{P}\check{\eta}_3\check{P}^{-1}. \tag{E.3}$$

The function $\mathcal{Z}(\Theta)$ is defined, following again Nazarov, as

$$\mathcal{Z}(\Theta) = G_Q\sum_p \frac{T_p}{1+\frac{T_p}{2}(\Theta(\epsilon)-1)},$$

containing all the information regarding the transmission eigenvalues.

Use of eq. E.3 can be illustrated by switching to the Matsubara technique. The electric current is found from

$$I_M = -\,\mathrm{Im}\left[\frac{\pi}{2e}T\sum_{\zeta}\mathcal{Z}(\Theta)\sqrt{\Theta^2-1}\ \ \mathrm{Tr}(\hat{\eta}_3\hat{P}\hat{\eta}_3\hat{P}^{-1})\right].$$

Evaluating the trace gives

$$\mathrm{Tr}(\hat{\eta}_3\hat{P}\hat{\eta}_3\hat{P}^{-1}) = \frac{F_1F_2^\dagger - F_2F_1^\dagger}{\sqrt{\Theta^2-1}}.$$

The expression for the current is then

$$I_M = -\,\mathrm{Im}\left[\frac{\pi}{2e}T\sum_{\zeta}\mathcal{Z}(\Theta)\ (F_1F_2^\dagger - F_2F_1^\dagger)\right].$$

Assuming equal superconducting reservoirs, the Matsubara Green's functions are

$$G^M_{1,2} = \frac{i\zeta_n}{\Omega};\quad F^M_{1,2} = \frac{|\Delta|\mathrm{e}^{(\mp \mathrm{i}\phi/2)}}{\Omega},$$

where $\Omega = i\sqrt{\zeta_n^2+|\Delta|^2}$. These give that

$$F_1F_2^\dagger - F_2F_1^\dagger = \frac{-2i|\Delta|^2\sin\phi}{\zeta_n^2+|\Delta|^2},$$

and that

$$\Theta = G_1G_2 + \frac{1}{2}(F_1F_2^\dagger + F_1^\dagger F_2) = \frac{\zeta_n^2+|\Delta|^2\cos\phi}{\zeta_n^2+|\Delta|^2}.$$

Using this expression for Θ, the function $\mathcal{Z}(\Theta)$ simplifies to

$$\mathcal{Z}(\Theta) = G_Q\sum_p \frac{(\zeta_n^2+|\Delta|^2)T_p}{\zeta_n^2+|\Delta|^2(1-T_p\sin^2(\phi/2))}.$$

The expression for the spectral current density is now

$$I_M = \frac{\pi T}{e}G_Q\sin\phi\sum_{p,\zeta}\frac{|\Delta|^2T_p}{\zeta_n^2+|\Delta|^2(1-T_p\sin^2(\phi/2))}.$$

Performing the summation over Matsubara freqencies ζ_n recovers the general current relation for a connector between two equal superconductors at equilibrium:

$$I_M = \frac{\pi}{2e}\sum_p \frac{G_QT_p|\Delta|\sin\phi}{\sqrt{1-T_p\sin^2(\phi/2)}}\tanh\left(\frac{|\Delta|}{2T}\sqrt{1-T_p\sin^2(\phi/2)}\right).$$

The energy spectrum can be found directly from the poles of $\mathcal{Z}(\Theta)$. They are

$$i\zeta \to E = \pm|\Delta|^2\sqrt{1-T_p\sin^2(\phi/2)},$$

the Andreev levels.

Bibliography

[1] J. Bardeen, L. N. Cooper, and J. R. Schrieffer, "Theory of superconductivity," *Phys. Rev.*, vol. 108, pp. 1175–1204, Dec 1957.

[2] J. Waldram, *Superconductivity of Metals and Cuprates*. Institute of Physics Pub.(Bristol and Philadelphia, Pa.), 1996.

[3] P. G. De Gennes, *Superconductivity of Metals and Alloys*. WA Benjamin, Inc., New York, 1966.

[4] J. R. Schrieffer, *Theory of Superconductivity*. Benjamin (New York), 1964.

[5] A. A. Abrikosov, L. P. Gor'kov, and I. Dzyaloshinskii, *Methods of Quantum Field Theory in Statistical Physics*. Pergamon (London), 1963.

[6] K. Usadel, "Generalized diffusion equation for superconducting alloys," *Physical Review Letters*, vol. 25, no. 8, pp. 507–509, 1970.

[7] Y. V. Nazarov, "Circuit theory of andreev conductance," *Physical review letters*, vol. 73, no. 10, pp. 1420–1423, 1994.

[8] Y. V. Nazarov, "Novel circuit theory of andreev reflection," *Superlattices and microstructures*, vol. 25, no. 5-6, pp. 1221–1231, 1999.

[9] Y. V. Nazarov and Y. M. Blanter, *Quantum transport*. Cambridge University Press, 2009.

[10] I. O. Kulik and A. N. Omel'Yanchuk, "Contribution to the microscopic theory of the josephson effect in superconducting bridges," *Soviet Journal of Experimental and Theoretical Physics Letters*, vol. 21, p. 96, 1975.

[11] J. Rammer and H. Smith, "Quantum field-theoretical methods in transport theory of metals," *Reviews of modern physics*, vol. 58, no. 2, pp. 323–359, 1986.

[12] J. W. Serene and D. Rainer, "The quasiclassical approach to superfluid 3he," *Physics Reports*, vol. 101, no. 4, pp. 221–311, 1983.

[13] V. Chandrasekhar, "Proximity-coupled systems: Quasiclassical theory of superconductivity," in *Superconductivity* (K. H. Bennemann and J. B. Ketterson, eds.), vol. 1, ch. 8, Springer, Berlin, 2004.

[14] L. Pitaevskii, "Phenomenology and microscopic theory: Theoretical foundations," in *Superconductivity* (K. H. Bennemann and J. B. Ketterson, eds.), vol. 1, ch. 2, Springer, Berlin, 2004.

[15] W. Belzig, F. K. Wilhelm, C. Bruder, G. Schön, and A. D. Zaikin, "Quasiclassical green's function approach to mesoscopic superconductivity," *Superlattices and Microstructures*, vol. 25, no. 5-6, pp. 1251–1288, 1999.

[16] G. Eilenberger, "Transformation of gorkov's equation for type ii superconductors into transport-like equations," *Zeitschrift für Physik A Hadrons and Nuclei*, vol. 214, no. 2, pp. 195–213, 1968.

[17] A. Shelankov, "On the derivation of quasiclassical equations for superconductors," *Journal of low temperature physics*, vol. 60, no. 1, pp. 29–44, 1985.

[18] M. Y. Kuprianov and V. F. Lukichev *Sov. Phys. JETP*, vol. 67, p. 1163, 1988.

[19] K. K. Likharev, "Superconducting weak links," *Reviews of Modern Physics*, vol. 51, no. 1, p. 101, 1979.

[20] A. A. Golubov, M. Y. Kupriyanov, and E. Il'Ichev, "The current-phase relation in josephson junctions," *Reviews of modern physics*, vol. 76, no. 2, p. 411, 2004.